國立臺灣大學醫學院生理學研究所博士論文

Graduate Institute of Physiology,

National Taiwan University College of Medicine

Doctoral Dissertation

腸道葡萄糖授予缺氧上皮細胞抗死亡之訊息傳遞路徑探討

Enteral glucose confers anti-death signaling in epithelial cells under hypoxic stress

黃菁英

Ching-Ying Huang

指導教授：余佳慧 博士

Linda Chia-Hui Yu, Ph.D

中華民國 102 年 5月

May 2013

目　　錄

口試委員會審定書

國立臺灣大學博士學位論文口試委員會審定書

中文題目：腸道葡萄糖授予缺氧上皮細胞抗死亡之訊息傳遞路徑探討

英文題目：Enteral glucose confers anti-death signaling in epithelial cells under hypoxic stress

本論文係黃菁英君（D95441005）在國立臺灣大學生理學研究所完成之博士學位論文，於民國 102 年 5 月 22 日承下列考試委員審查通過及口試及格，特此證明

口試委員：李佳慧（簽名）

（指導教授）

邱明燈

劉秉彥　賴逸儒

李碧惠

系主任、所長　湯志永（簽名）

Acknowledgement

這本論文的完成，首先要向恩師余佳慧老師致上最崇高的謝意，在余老師的引領之下，讓我在腸胃道生理學的領域之中，享受科學研究的樂趣。在博士班的期間，無論是研究方法的設計或論文撰寫與修改，總可以在老師的悉心指導之下獲得新的啟發，愈加喜愛研究工作。也因為時常受到余老師以正面積極的態度鼓舞，使我在研究的挫敗之中，能依舊擁有熱忱，而老師也一直是我所學習與景仰的典範。對於余老師的感謝難以在三言兩語中表達，在學術研究的路上，將永遠感激在心。

感謝口試委員林明燦老師、許秉寧老師、賴逸儒老師與梁碧惠老師。對論文的細心匡正與指導，使論文更臻完整。謝謝參與兩篇畢業論文完成的蕭仲凱醫師、盧彥臻、張哲堯、郭瑋庭、黃怡禎與李宗錞醫師，因為你們的幫助，讓研究得以順利進行。謝謝所上老師平日的教導與協助；也感謝所上職員與助教在行政事務與庶務上的幫忙和熱心提醒。感謝曾經共處在腸胃道生理所研究室的所有夥伴們，無論是日常與實驗上的幫助，或是在你們身上學習與分享的事物，都令人感激!

有太多未能一一道盡的感謝，謹在此謝謝所有一路相伴的友情、愛情與親情！你們是我生命中最珍貴的瑰寶。

Abstract in Chinese (中文摘要)

腸胃道受缺血或低氧壓力引發之上皮細胞死亡調節失常現象，與器官功能異常和腫瘤生成有關。先前的研究發現，腸道葡萄糖可透過未知機制授予腸道上皮細胞抗死亡之能力。活化第一型鈉-葡萄糖轉運蛋白(sodium/glucose transporter 1 ，SGLT1)可避免腸道上皮細胞因微生物刺激而走向細胞凋亡。除此之外，有文獻記載在人類大腸直腸癌細胞的壞死區域周圍，葡萄糖轉運蛋白(Glucose transporters, GLUTs) 的異常表現會伴隨低氧誘發因子(Hypoxia inducicle factor (HIF)1α)共存，推論葡萄糖攝取增加與缺氧區域之抗壞死有關。第一部份之研究目的，欲透過動物實驗探討腸腔中葡萄糖對腸繫膜缺血造成之上皮細胞死亡與腸道屏障功能失常之保護作用，並進一步研究葡萄糖所媒介之細胞生存訊息傳遞路徑。第二部分之研究目的，則利用人類大腸直腸癌細胞株，探討缺氧誘發細胞計畫性壞死之訊息傳遞路徑，以及葡萄糖代謝物丙酮酸在細胞死亡阻抗性中所扮演的角色。

在第一部份的實驗中發現，將上腸繫膜動脈夾閉造成缺血刺激，會快速引發空腸上皮細胞凋亡。而缺血後再灌流，則造成凋亡蛋白酶依賴性之腸道通透性上升，腸道細菌轉移增加，以及腸黏膜發炎。腸道葡萄糖經由 SGLT1 攝取，降低缺血再灌流引發之上皮細胞凋亡、屏障受損，以及黏膜發炎；其乃藉由活化抗凋亡之 PI3K/Akt 路徑及其下游訊息傳遞分子，包括磷酸化 mTOR 與 Bad 蛋白，去磷酸化 p38 MAPK 蛋白。

在第二部份的實驗中，將人類大腸直腸癌細胞暴露於缺乏氧氣與葡萄糖之環境中，可誘發其發生計劃性壞死，包括 receptor-interacting protein kinase (RIP)依賴性乳酸去氫酶之滲漏與 RIP1/3 複合體生成。缺氧刺激後亦誘發粒線體中超氧化物產生；而給予抗氧化物之後則可抑制 RIP 訊息與細胞壞死。RIP 依賴性之計畫性壞死，在給予葡萄糖後消失；但若將葡萄糖以其他非代謝性醣類似物取代則無此效果。缺氧細胞在給予葡萄糖後 HIF1α 有轉移細胞核的現象，且與 GLUT1 與 GLUT4 之表現增加具關聯性。醣解代謝授予缺氧癌細胞對計劃性壞死之阻抗性，乃部分源自於丙酮酸清除粒線體自由基的作用且不需依賴能量生成

總括而論，我們發現給予腸道葡萄糖可降低因缺氧壓力造成之細胞凋亡或計畫性壞死，其抗死亡之作用乃分別透過活化抗凋亡之 PI3K/Akt 訊息傳遞路徑；或是經由丙酮酸對粒線體自由基之清除作用。

Abstract

Dysregulated epithelial cell death caused by ischemic or hypoxic stress is associated with malfunction or tumorigenesis in gastrointestinal tract. Previous studies have shown that enteral glucose uptake confers resistance to epithelial cell death via unknown mechanisms. Activation of sodium/glucose transporter 1 (SGLT1) prevented epithelial apoptosis caused by microbial products. In addition, abnormally expressed glucose transporters (GLUTs) were found colocalized with hypoxia inducible factor (HIF)1α in peri-necrotic regions in human colorectal carcinoma, suggesting that enhanced glucose uptake may be linked with anti-necrotic resistance in hypoxic tumor core. The aim of the first study was to explore whether luminal glucose uptake protects against mesenteric ischemia-induced epithelial cell death and intestinal barrier dysfunction, and to explore the glucose-mediated cellular survival pathways *in vivo*. The aim of the second study is to investigate signaling pathways of hypoxia-induced necroptosis and explore the role of glucose pyruvate metabolite in mechanisms of death resistance in human colorectal cancer cells.

In the first part of study, ischemic challenge by occlusion of superior mesenteric artery caused rapid onset of enterocyte apoptosis in rat jejunum. Ischemia-reperfusion (I/R) triggered rise of intestinal permeability, augmentation of bacterial translocation

(BT) and mucosal inflammation in a caspase-dependent manner. SGLT1-mediated enteral glucose attenuated I/R-induced epithelial apoptosis, barrier damage, and mucosal inflammation via activation of anti-apoptotic PI3K/Akt signaling, including phosphorylation of mTOR and Bad, and dephosphorylation of p38 MAPK.

In the second part of study, human colorectal carcinoma cells hypoxia exposed in glucose-free media displayed signs of necroptosis, including receptor interacting protein (RIP)-dependent lactodehydrogenase leakage and RIP-1/3 complex formation. Generation of mitochondrial superoxide was noted after hypoxic challenge; its reduction by antioxidants inhibited RIP signaling and cell necroptosis. Addition of glucose and pyruvate derivative, but not non-metabolizable analogs, diminished RIP-dependent necroptosis. Hypoxic cells with glucose showed HIF1α activation and hypoxia-targeted gene (GLUT-1 and -4) expression. Glycolytic pyruvate scavenging of hypoxia-induced mitochondrial superoxide was involved in anti-necrotic mechanisms in an energy-independent manner.

In conclusion, we found that enteral glucose uptake attenuated both type of cell death, apoptosis and necroptosis in gut epithelial cell under hypoxic stress via either anti-apoptotic PI3K/Akt signaling pathway or through pyruvate scavenging of mitochondrial free radical, respectively.

Chapter 1 INTRODUCTION

Human gut mucosa serves as a barrier between external environment and internal milieu. The mucosal barrier includes a single layer of columnar epithelial cells connected by apical tight junctional complex, a hydrated gel layer formed by mucin covering the epithelial cells, and immune cells in lamina propria (Turner, 2009). The epithelial cells that prevents abnormal influx of noxious luminal contents is also responsible for nutrient uptake through apically expressed transporters (Laukoetter et al., 2006). In physiological conditions, commensal bacteria (~100 trillions) are restricted in the gut lumen and separated from the lamina propria by epithelial cells and mucus layers. However, abnormal translocation of bacteria to sterile extraintestinal visceral organs may occur under inflammatory situation and metabolic stress, resulting in sepsis and life-threatening complications(Yu et al., 2012).

1.1 Physiological hypoxia in the gut

The gut epithelium is anatomically positioned between an anaerobic lumen and a highly vascularized lamina propria. Despite rich blood supply to the intestine, a steep oxygen gradient was found along the crypt-villus axis where low oxygen concentration was seen at the villous tips. The term “physiological hypoxia” was used to describe gut

epithelial cells under an extremely low level of oxygenation acquire regulatory mechanisms to adapt to the shifted oxygen gradient (Colgan et al., 2010).

1.2 Pathological hypoxia in the gut

Mesenteric ischemia/reperfusion (I/R) is seen in patients with mesenteric artery embolism, strangulated hernias, and in neonatal necrotizing enterocolitis. It also seen in the case of major abdominal and vascular surgery or collapse of systemic circulation occurred by traumatic or hemorrhage shock (Mallick et al., 2004; Yasuhara, 2005; Yu, 2010). The disruption of blood supply during ischemia reduces oxygen and nutrient supply to mucosal cells. The production of free radicals stimulated by subsequent restoration of blood flow causes further oxidative stress, which increases inflammation and aggravates tissue damage (Nilsson et al., 1994; Mallick et al., 2004; Yu, 2010). One of the major consequences of mesenteric I/R is heightened mucosal cell death and gut barrier damage, leading to enteric bacterial translocation and septic complications. Both modes of cell death, apoptosis and necrosis, were observed in the gut mucosa upon mesenteric I/R injury (Wu et al., 2004; Aban et al., 2005; Chang et al., 2005).

1.3 Hypoxia in colorectal cancer

Rapid cell growth and poorly formed vasculature characterized in malignant cancers are often accompanied by a hypoxic microenvironment in the tumor core (Brown and

Giaccia 1998; Milosevic, Fyles et al. 2004). Necrotic cell death has been reported in the hypoxic core in colorectal tumors due to depletion of oxygen and nutrients, However, malignant cells may develop adaptive mechanisms by metabolic reprogramming to survive under extremely deprived conditions, which is also related to tumor resistance to anticancer drugs (Hawley et al., 1992).

1.4 Modes of cell death

Cell apoptotis (programmed cell death) is characterized by caspase-dependent signaling pathways and nuclear DNA fragmentation. The signaling pathway of apoptosis may be triggered extrinsically via Fas or TNF receptors, or intrinsically via mitochondrial pathways, leading to caspase-3 cleavage and ultimately, endonuclease activation for oligonucleosome formation (Ramachandran et al., 2000). The Bcl-2 family (e.g., anti-apoptotic Bcl-2, Bcl-X_L, and pro-apoptotic Bax) are important regulators of mitochondrial-dependent apoptosis (Mayer et al., 2003). The mitochondrial undergo an increase in membrane permeability and a reduction of membrane potential accompanied by cytosolic release of cytochrome *c*. The release of cytochrome *c* from mitochondria can be blocked by anti-apoptotic protein Bcl-2, while the translocation of pro-apoptotic Bax from cytosol bound to mitochondria induces cytochrome *c* release during apoptosis. The released cytochrome c binding to an apoptosis binding factor-1 forms apoptosomes

to activate caspase-9. (Shimizu et al., 1999; Zheng et al., 2004). Morphological changes, such as cell shrinkage, membrane blebbing, and chromatin condensation, are seen in cells that undergo apoptosis (Ramachandran et al., 2000).

On the other hand, necrotic cell death has been traditionally regarded as an uncontrolled form of cell death. Cell necrosis is characterized by morphological alteration, i.e. cytoplasmic swelling, subcellular organelle breakdown, loss of plasma membrane integrity and release of cellular contents. Most research of necrotic death in enterocytes is based on morphological and biochemical analysis (Chakrabarti et al., 2003; Jilling et al., 2006; Higa et al., 2007; Kalischuk et al., 2007; Hunter et al., 2008; Vincenti et al., 2010). Recent data from human intestinal epithelial HT-29 cells, lymphocytes, monocytes and fibroblasts have indicated that signaling molecules such as receptor-interacting proteins (RIPs) are involved in necrotic mechanisms triggered by cytotoxic agents such as tumor necrosis factor (TNF) (Meurette et al., 2007; Declercq et al., 2009; He et al., 2009). The formation of RIP1-RIP3 complex followed by auto- or mutual phosphorylation of RIP proteins is associated with mitochondrial bioenergetic alterations and intracellular ATP decline in cells undergoing programmed necrosis (Temkin et al., 2006; Cho et al., 2009; Zhang et al., 2009; Berghe et al., 2010). Reactive oxygen species (ROS) derived from the mitochondrial respiratory chain has also been implicated in necrotic mechanisms (Declercq et al., 2009; Zhang et al., 2009). To date,

the involvement and cascading order of these necrotic effectors in ischemic or hypoxic enterocytes remain unclear.

1.5 Role of glucose in death resistance

Several lines of evidence indicated that presence of glucose may inhibit cell death in intestinal epithelial cells. Previous studies demonstrated that sodium-dependent glucose uptake protects intestinal cells against apoptosis caused by bacterial lipopolysaccharide and parasitic products (Yu et al., 2005; Yu et al., 2006; Yu et al., 2008). Increased levels of anti-apoptotic Bcl-2 and Bcl-xL were noted following activation of apically expressed sodium-glucose transporter (SGLT)-1 (Yu et al., 2005). A more recent report showed that initiation of Na^+-glucose cotransport by SGLT1 triggered downstream Akt signaling for regulation of cellular functions (Shiue et al., 2005). A critical role of PI3K/Akt signaling in resistance to apoptosis has been reported in multiple cell types (Chang et al., 2003; Bouchard et al., 2008). Studies have shown that PI3K/Akt phosphorylates and thereby inactivates Bad (a pro-apoptotic mitochondrial Bcl-2 family protein) or phosphorylates mTOR that then activates $p70^{S6K}$ to phosphorylate Bad (Chang et al., 2003; Bouchard et al., 2008). Other downstream targets of Akt that are involved in regulating cell survival and cell cycle progression include IκBα/NFκB, glycogen synthase kinase 3 (GSK3), and Forkhead family of transcription factors

(FoxOs) (Liang et al., 2003; Urbich et al., 2005; Dan et al., 2008; Bai et al., 2009).

One of the pro-survival mechanisms in tumor cells is by metabolic reprogramming for high levels of glycolysis. The term “Warburg’s effect” describes the phenomenon that over fifty percent of cellular energy is produced by glycolysis in the tumor in compared to that ninety percent of energy is produced by mitochondrial oxidative phosphorylation in normal tissues (Warburg, 1956). Moreover, a large body of evidence shows that upregulation of glycolytic enzymes and glucose transporters (GLUTs) are linked to transcription activity of hypoxia inducible factor (HIF) 1α triggered by low oxygen condition (Yeh et al., 2008; Chiacchiera et al., 2009; Marin-Hernandez et al., 2009). Recent reports documented that HIF1α and GLUT-1 colocalize at peri-necrotic regions in human colorectal tumors (Greijer et al., 2008; Airley et al., 2010), suggesting that glucose metabolism may confer anti-necrotic resistance to hypoxic stress. Glucose is catalyzed to ATP and pyruvate by a cascade of glycolytic enzymes, such as glucokinase and glyceraldehyde-3-phosphate dehydrogenase (GPD)(Fleming et al., 1997). The final glycolytic product pyruvate is also the starting substrate for tricarboxylic acid (TCA) cycle after being transported across inner mitochondrial membrane by mitochondrial pyruvate carrier (MPC) (Hildyard et al., 2005; Herzig et al., 2012). Aside from its critical role as the link between glycolysis and mitochondrial respiration, pyruvate also scavenges ROS through a non-enzymatic reaction (Kao et al.,

2010). Numerous studies have suggested that chemoresistance may be due in part to glycolytic ATP as a preferential energy source for promoting cancer cell survival (Xu et al., 2005), (Zhou et al., 2012).

To date, whether enteric glucose uptake prevents epithelial cell death caused by mesenteric I/R or hypoxic stress remains unclear. Moreover, molecular mechanisms of glucose-mediated resistance to cell apoptosis and necrosis have yet to be explored.

1.6. Aim of the study

In the current study, we explored whether enteral glucose confer anti-death signaling against hypoxic stress in rat intestinal I/R or in human colorectal cancer line.

Chapter 2 MATERIAL & METHODS

Intestinal ischemia/reperfusion

Male Wistar rats (250–300 g) were raised in a temperature-controlled room with 12-hr light-dark cycles, and fed regular rat chow and water. Rats were fasted overnight with free access to water, and subjected to sham operation or mesenteric I/R challenge. In I/R rats, the superior mesenteric artery (SMA) was occluded with an atraumatic microvascular clamp for 20 minutes and then released for up to 60 minutes. Ischemia of the bowel was verified by the loss of mesenteric pulsations and bluish discoloration of the jejunum. Sham controls rats received mock manipulation of SMA without occlusion. All animals were placed on heating pads to maintain body temperature at 37°C during the operation, and the heart rate was closely monitored. All protocols used in this study were approved and monitored by the Institutional Animal Care and Use Committee, National Taiwan University.

Experimental design

The experimental protocols were carried out under aseptic conditions. After anesthetization with urethane (1.2 g/kg, intraperitoneal injection; Sigma-Aldrich, MO), all rats were subjected to midline laparotomy and a 10-cm jejunal sac was created by

thread ligature at both ends, beginning 10 cm distal to the ligament of Treitz in each animal. Care was taken not to occlude or puncture mesenteric vessels during the ligation. A 1 ml syringe with a PE-10 catheter was intubated to one end of the jejunal sac and 0.5 ml of Krebs buffer with the pancaspase inhibitor ZVAD (EMD Chemicals Inc., Darmstadt, Germany) or glucose (Sigma) was carefully injected into the lumen. The formula for Krebs buffer was 115 mM NaCl, 8 mM KCl, 1.25 mM $CaCl_2$, 1.2 mM $MgCl_2$, 2.0 mM $KHPO_4$, 25 mM $NaHCO_3$, pH 7.33 - 7.37. Animals were then subjected to sham operation or I/R challenge as described above.

Rats were randomly assigned to six groups (n = 6-8 / group): Group 1, sham controls that underwent laparotomy and whose jejunal lumen was instilled with Krebs buffer before sham operation; Group 2, sham+Z rats that underwent laparotomy and whose jejunal lumen was instilled with 120 μM ZVAD in Krebs buffer 30 minutes prior to sham operation; Group 3, sham+G rats that were enterally administered 25 mM glucose in Krebs buffer immediately before sham operation; Group 4, I/R rats that were enterally instilled with Krebs buffer before SMA occlusion for 20 minutes and reperfusion for 60 minutes; Group 5: I/R+Z rats that were enterally instilled with 120 μM ZVAD in Krebs buffer 30 minutes prior to the same I/R procedure; and Group 6: I/R+G rats that were enterally administered 25 mM glucose in Krebs buffer immediately before I/R challenge. The concentrations of ZVAD and glucose used here have been

previously shown to inhibit cell apoptosis induced by microbial products in epithelial cell cultures (Yu et al., 2005; Yu et al., 2008).

In some experiments, phloridzin (a SGLT1 inhibitor; 0.5 - 2.5 mM) and phloretin (a GLUT2 inhibitor; 1.5 and 2.5 mM) were added to the glucose solution for enteral instillation prior to the I/R procedure. In addition, to investigate the involvement of PI3K in the signaling pathways of glucose-mediated rescue mechanism, LY294002 (10 mg/kg) and wortmannin (7.5 μg/kg) were administered intraperitoneally and intravenously, respectively, 30 minutes before I/R challenge in the presence of luminal glucose. At the end of the surgical procedures, the jejunal tissues, the liver, and the spleen were collected for experimental analysis.

Histopathological scoring

Jejunal segments were fixed in 4% paraformaldehyde, and care was taken to ensure proper orientation of the crypt to villus axis during embedding. Sections of 4 μm thickness were stained with hematoxylin and eosin (H&E). The degree of intestinal injury was evaluated using a light microscope and graded by two independent persons blind to the actual treatment. Briefly, intestinal injury was scored from 0 to 5 according to the following criteria: grade 0, normal mucosal villous structure; grade 1, presence of subepithelial space at villous tips; grade 2, scattered epithelial denudation on villous tips;

grade 3, denuded tips with exposed lamina propria and villous blunting; grade 4, epithelial shedding from both the apex and mid-region of the villi associated with shortened and widened villous structure; grade 5, complete destruction of villi and disintegration of lamina propria with ulceration.

TUNEL assay

Paraffin-embedded jejunal sections were deparaffinized and *in situ* detection of cells with DNA-strand breaks was performed by the TUNEL labeling method using a TdT-FragEL™ DNA fragmentation detection kit (Oncogene Research Products, Boston, MA) following the manufacturer's protocol. Negative controls were performed by substituting tris-buffered saline (TBS) for the TdT enzyme.

Caspase-3 activity assay

Scraped jejunal mucosa was lysed and the protein concentration of the lysate was adjusted to 50 μg/ml to test for caspase-3 activity (Anaspec, San Jose, CA). The assay is based on spectrophotometric detection of the chromophore rhodamine 110 (Rh110) after cleavage from the labeled substrate DEVD-Rh110. The caspase-3 activity of samples was measured in relative fluorescence units (RFUs) at Ex/Em = 496 nm/520 nm for 60 minutes in 5-minute intervals. The level of caspase-3 activity was expressed as

RFU/min/mg.

Ussing chamber studies and macromolecular flux assay

Intestinal segments were excised and immediately placed in warm Krebs buffer. The external muscle layers were stripped off, leaving the submucosal plexus and mucosa intact. From each rat, two pieces of the muscle-stripped tissues (cut longitudinally into flat sheets along the mesenteric border) were mounted in Ussing chambers (WPI Instruments, Sarasota, FL). Care was taken to avoid tissues containing Peyer's patches. The opening area (2 cm^2) of the chamber exposed the tissue to 5 ml of circulating oxygenated Krebs buffer. The serosal buffer contained 10 mM glucose that was osmotically balanced with 10 mM mannitol in the mucosal buffer. A circulating water bath maintained the temperature of the buffer at 37°C. The serosal and mucosal tissue baths were clamped at 0 V using a voltage clamp feedback amplifier (WPI Instruments). The short-circuit current (Isc, $\mu A/cm^2$) of the tissue was recorded continuously on line. At 5-minute intervals, the voltage between the two baths was stepped to 1 mV for one second, and the change in the Isc caused by the pulse was used to calculate the tissue conductance (mS/cm^2) according to Ohm's law (Yu et al., 2003).

The intestinal epithelial permeability was determined by the level of mucosal-to-serosal flux of horseradish peroxidase (HRP type II, MW = 44 kD, Sigma).

Tissues in the Ussing chambers were allowed to equilibrate until the Isc stabilized before HRP was added to the luminal buffer at a final concentration of 5×10^{-5} M. Samples (300 μl) of serosal buffer were collected at 0, 30, 60 and 90 minutes after luminal addition of HRP, and were replaced with Krebs buffer. The concentration of HRP was determined by a kinetic enzymatic assay. Fluxes were calculated according to standard formulae and were expressed as pmol/cm^2/hr (Yu et al., 2003).

Fluorescein-based gut permeability assay

To assess gut permeability *in vivo*, a fluorescein-based assay was performed as described previously with slight modification (Wang et al., 1998). The 4-kDa fluorescein isothiocyanate-conjugated dextran (FD4, Sigma) dissolved in Krebs buffer was administered into the lumen of ligated jejunal sac to a final concentration of 0.5 mg/ml immediately after the release of the artery clamp. The jejunal sac was placed back into the peritoneal cavity, and the open abdomen was covered with a saline-wetted gauze and foil to prevent evaporation and direct light. Arterial plasma from 0.5 ml of blood was taken at 60 minute post-reperfusion. Fluorescence intensity in arterial plasma was measured at Ex/Em = 496/520 nm using a plate reader. The concentration (μg/ml) of FD4 in plasma was calculated using a standard curve.

Magnetic Resonance Imaging (MRI)-based gut permeability assay

To assess gut permeability *in vivo*, the contrast agent gadodiamide (Omniscan, GE Healthcare) was instilled into the lumen of the ligated jejunal sac to a final concentration of 0.25 M immediately after the release of the artery clamp, and the signal intensity of this agent in the liver and kidney was quantified using abdominal MRI as described previously (Hsiao et al., 2009). In sham controls, gadodiamide was injected into the jejunal sac after mock manipulation. The rats were placed in a home-made resonance coil with inner diameter of 6 cm, and abdominal MRI was performed at various time points (0, 5, 10, 15, 30, 45 and 60 minutes) using a clinical 1.5 T MR System (Signa Excite; GE Healthcare). Two dimensional T1-weighted fast spin echo MRI pulse sequences were used, with the following parameter set: TR/TE = 140/4.2 msec, FOV = 12 × 8.4 cm^2, and NEX = 4. The signal intensity produced by gadodiamide in the region of interest (ROI), liver and both kidneys, was measured. Signal-to-noise ratio (SNR) was calculated by dividing the signal intensity of the ROI by that of the background. To quantify the gadodiamide delivered to the systemic circulation, samples of plasma from 0.5 ml of blood taken before (t = 0 minutes) and 15, 30, and 60 minutes after injecting gadodiamide were prepared. A known concentration (0.5 M) of gadodiamide solution was serially diluted with neat plasma to prepare standard solutions for the calibration curve. Plasma and standard solutions were

subjected to MRI scan, and imaging parameters were: TR/TE = 550/67.50 msec, FOV = 14 × 0.5 cm^2, and NEX = 4. The SNRs of the standard solutions of gadodiamide were plotted against their respective concentrations to establish a standard curve. The plasma gadodiamide concentrations were calculated from the standard curve (Hsiao et al., 2009).

Analysis of bacterial translocation

The liver and spleen tissues were homogenized, sonicated and adjusted to a protein concentration of 0.1 g/ml with sterile PBS. Each homogenate was inoculated onto fresh blood agar plates (200 μl per plate; Scientific Biotech Corp., Taipei, Taiwan) and the plates were incubated at 37°C overnight. The number of bacterial colony forming units (CFU) was normalized per gram of tissue (CFU/g).

Myeloperoxidase (MPO) activity assay

Intestinal samples were homogenized and sonicated in 10 volumes of potassium phosphate buffer (PPB, 50 mM, pH 6.0) containing 0.5% HTAB (Sigma). Lysates were centrifuged and supernatants were diluted in PPB containing 0.167 mg/ml of O-dianisidine dihydrochloride (Sigma) and 0.0005% of H_2O_2. The enzyme concentration was determined from the absorbance at 460 nm measured every 30

seconds over a 5 minute period. One unit of MPO activity was defined as the quantity of enzyme degrading 1 μmol of H_2O_2 per minute, and MPO activity of the gut was expressed in U/mg of tissue.

ELISA for TNFα and MIP-1α

Scraped jejunal mucosa were homogenized and sonicated in PBS and the lysate was centrifuged. The protein concentration in the supernatant was quantified. The levels of TNFα and MIP-1α in mucosal samples were measured by using ELISA development kits (PeproTech, NJ) according to the manufacturer's instructions. To measure cytokine levels, microplates were coated overnight with capture antibodies. The plates were blocked with PBS containing 1% BSA for 1 hour and washed. The sample and standard solutions were added and incubated for 2 hours. The biotinylated antigen-affinity detection antibodies were incubated for another 2 hours. After washing, avidin-HRP conjugate was added for 30 minutes followed by incubation with ABTS liquid substrate for color development. Absorbance was measured at 405 nm with correction set at 650 nm. The cytokine levels in jejunal mucosa were expressed in pg/mg of protein.

Immunohistochemical and immunofluorescence staining for rat jejunal tissue

Tissue sections were incubated with 3 % H_2O_2 to block endogenous peroxidase for

immunohistochemical staining and were quenched with 50 mM NH_4Cl in PBS for immunofluorescence staining, and then blocked with 2% normal goat serum. Tissue sections were incubated with anti-cleaved caspase-3 (1:1000 Cell signaling, Danvers, MA), anti-proliferating cell nuclear antigen (PCNA) (1:100, Lifespan biosciences, Seattle, WA), anti-SGLT1 (1:200, Millipore, Billerica, MA), anti-Akt (1:100, Cell signaling), or isotype control antibodies. After washing with PBS, tissues stained for SGLT1 were incubated with biotin-conjugated goat anti-rabbit IgG (1:1000, Molecular Probes, Carlsbad, CA) for one hour, followed with a streptavidin-conjugated Alexa Fluor® 488 fluorescent probe (1:1000, Molecular Probes) for one hour; tissues stained for Akt were incubated with goat anti-mouse IgG conjugated to Alexa Fluor® 488 fluorescent probe (1:1000, Molecular Probes) for one hour. All tissues were stained with Hoechst dye to visualize cell nuclei. Tissues stained for cleaved caspase-3 and PCNA were incubated with HRP-conjugated SignalStain® Boost anti-rabbit IHC detection reagent (Cell signaling) and developed with a DAB peroxidise substrate followed by counterstain with hematoxylin. The slides were mounted with aqueous mounting media and viewed under a Zeiss fluorescence microscope.

Western blotting for jejunal mucosa

Scraped jejunal mucosa was homogenized in ice-cold complete RIPA buffer, and

the lysate was sonicated and centrifuged. The protein concentration of the supernatant was adjusted to 5 mg/ml and diluted at a 1:1 vol:vol ratio in 2× electrophoresis sample buffer containing 2% (w/v) SDS, 100 mM DTT, and 62.5 mM Tris/HCl (pH 6.8). Samples were then heated to 95°C in a heat block for 5 minutes, and stored at –20°C until used for immunoblotting.

The extracted proteins were separated by SDS-PAGE, and the resolved proteins were electrotransferred onto membranes. After blocking with 5% non-fat milk in TBS, the membrane was incubated with anti-occludin (1:1000, Invitrogen), anti-Akt (1:500, Cell signaling), anti-phospho-Akt (1:1000, Cell signaling), anti-IκBα (1:1000, Santa Cruz, Santa Cruz, CA), anti-phospho-IκBα (1:1000, Santa Cruz), anti-phospho-Bad (1:500, Cell signaling), anti-phospho-mTOR (1:500, Cell signaling), anti-phospho-GSK3α/β (1:1000, Cell signaling), or anti-phospho-FoxO1/3a (1:1000, Cell signaling) at 4°C overnight. A monoclonal mouse anti-β-actin (1:10000, Sigma) was also used to control for equal loading in each sample. Membranes were washed with 0.1% Tween 20 in TBS and incubated with either horseradish peroxidase-conjugated goat anti-rabbit or anti-mouse IgG (1:1000, Cell signaling). The antigens were revealed and band density quantified by photoimage analysis.

Akt kinase activity

The kinase activity of Akt was determined using a non-radioactive Akt kinase assay kit (Cell signaling) according to the manufacturer's instruction. Briefly, scraped jejunal mucosa was homogenized in ice-cold lysis buffer, and the lysate was sonicated and centrifuged. For immunoprecipitation, 20μl of immobilized antibody beads conjugated to anti-phospho-Akt was added to 200μl of cell lysate (the protein concentration was 2.25 mg/ml) with gentle rocking overnight at 4°C. After washing with lysis buffer and kinase buffer, the pellet was incubated with ATP and GSK3 fusion protein for 30 minutes for kinase reaction. Exogenous GSK3, a downstream target of Akt, served as the substrate of phospho-Akt in this assay. The reaction was terminated by addition of 2× SDS sample buffer. The Akt kinase activity was determined by Western blot using anti-phospho-GSK3α/β antibody.

Cell culture models

Human colonic carcinoma Caco-2 and HT29 cells were grown in Dulbecco's modified Eagle's medium (DMEM; Invitrogen, Grand Island, NY, USA) containing 5 mM glucose and without pyruvate (Kles et al., 2002; Yu et al., 2005). The media was supplemented with 10% fetal bovine serum, 15 mM HEPES, 100 U/mL penicillin, and 0.1 mg/mL streptomycin (Sigma, St. Louis, MO, USA). Cells were seeded in 96- well (105 cells/well) or 24-well (106 cells/well) tissue culture plates (Costar, Corning, NY,

USA). Cells were grown to confluency for one week at 37 °C with 5% CO2 and 96% humidity. In all studies, cells were used between passages 21 and 27.

Hypoxic challenge and glucose deprivation

Cells were deprived of oxygen and glucose as previously described (Kalda et al., 1998; Kles et al., 2002; Shahrzad et al., 2005). Hypoxic (Hx) challenge was conducted using a modular incubator chamber (Billups-Rothenberg, CA, USA) by infusion of 5% CO2 and 95% N2 at 10 L/min for 5 minutes; normoxic (Nx) controls were kept at 5% CO2 and 95% air (Kalda et al., 1998; Kles et al., 2002; Shahrzad et al., 2005). In some groups, cells were pretreated with necrostatin-1 (Nec-1; a specific RIP1 inhibitor), BHA (200 μM; a free radical scavenger), apocynin (1 mM; an inhibitor to NADPH oxidase), or vehicle controls prior to hypoxic challenge to examine cell death pathways.

In additional experiments, cells were incubated in glucose-free and pyruvate-free DMEM media (Invitrogen) supplemented as above plus 0-25 mM glucose. To verify the role of glycolysis in death resistance, cells were pretreated with inhibitors to the cascade of glucose metabolic pathways such as IA (1 mM; a glycolytic inhibitor to GPD) and UK (10 μM; a MPC inhibitor), or with vehicle controls prior to hypoxic challenge in the presence of glucose. In another set of experiments, equimolar concentrations of substances were apically instilled in place of glucose to verify cellular metabolic status,

such as 3-O-methyl-glucopyranoside (3-OMG; a non-metabolizable sugar analog taken up by glucose transporters), mannitol (a non-absorbable and non-metabolizable sugar used as an osmolarity control), or glutamate (an amino acid used as an oxidative fuel control) before hypoxic challenge. The anti-necrosis effect of a cell-permeable pyruvate derivative, ethyl pyruvate (25 mM), was also examined in hypoxic cells. All reagents were purchased from Sigma.

Lactodehydrogenase (LDH) leakage assay

The leakage of intracellular enzyme LDH into the surrounding environment indicates rupture of plasma membrane, which is a hallmark of cell necrosis. The cell culture supernatant was collected after hypoxic challenge for the measurement of LDH activity. Briefly, a reaction mixture of 0.2 mM NADH and 0.36 mM sodium pyruvate was dissolved in Krebs-Henseleit (K-H) buffer containing 2% BSA. The K-H buffer is composed of 118 mM NaCl, 4.8 mM KCl, 1.2 mM MgSO4, 1.25 mM CaCl2, 1.2 mM KH2PO4, 24 mM NaHCO3 (pH7.4). Ten μl of cell supernatant and 190 μl of reaction mixture were mixed well in 96-well plates prior to spectrophotometric kinetic readings. Owing to the differences in the absorption spectra of NADH and NAD+, changes in the NADH concentration can be detected at 340 nm. The decrease in absorbance measured every minute over a 10-min period represents the activity of LDH. One unit of LDH

activity is defined as the quantity for oxidation of 1 μmole NADH per minute; the LDH activity of cell supernatant was expressed in Units per liter (Unit/L).

Analysis of mitochondrial functions by time-lapse microscopy

Mitochondrial transmembrane potential changes and ROS production were measured by using cell-permeant cationic fluorescent dyes, including 5,5',6,6'-tetrachloro-1.1',3,3'-tetraethylbenzimidazolylcarbocyanine iodide (JC-1) reagents and MitoSOX (Invitrogen, CA, USA) . The JC-1 reagent emits red fluorescence in its aggregated form when it accumulates in the negatively charged mitochondrial matrix of viable cells. The monomeric form of JC-1 emits green fluorescence when the dye is dispersed in the cytoplasm due to the loss of mitochondrial transmembrane potential. MitoSOX Red, which selectively targets functional mitochondria, exhibits red fluorescence after oxidization by superoxide. Cells grown on 96-well culture plates or 8-well chamberslides (2 x 105 cells/well, Costar) were incubated with JC-1 (10 μg/ml) or MitoSOX (5 μM) for 20 min, and washed twice prior to hypoxic challenge, and then subjected to fluoremetric readings. Alternatively, cells were analyzed by time-lapse microscopy using Application Solution Multi-Dimensional Workstation (AS MDW) (Leica Microsystems, Mannheim, Germany). Cells were loaded with JC-1 (10 μg/ml) for 30 min before infusion of 5% CO2 and 95% N2 into

the temperature-controlled moisture chamber of the AS MDW for live cell imaging.

Immunoprecipitation of RIP1-RIP3 complex and in vitro kinase assay

Cells lysates were immunoprecipitated with anti-human RIP1 (BD bioscience, Franklin Lakes, NJ, USA) overnight, and then incubated with protein G agarose beads for one hour at 4°C followed by centrifugation. The pellet was dissolved in electrophoresis sample buffer for heat denaturation. The immune complexes were subjected to reducing SDS/PAGE and the membranes were incubated with anti-RIP1 (1:1000, BD bioscience) or polyclonal rabbit anti-RIP3 (1:1000, Abcam, Cambridge, UK) for immunoblotting. For *in vitro* kinase assays, the bead pellets were incubated in kinase reaction buffer supplemented with 10 μM cold ATP and 1μCi γ-32P-ATP for 30 min at 30°C. The samples were resolved by SDS/PAGE and exposed to film for autoradiography as previously described (He et al., 2009).

RNAi-mediated knockdown of RIP1

RIP1 siRNA and negative control were purchased from Dharmacon, Lafayette, CA, USA. Cells were transfected with 100 nM siRNA oligonucleotides using DharmaFECT® siRNA transfection reagents as per manufacturer's protocol.

Knockdown efficiency of transfected cells was confirmed by western blotting 96 hrs post transfection.

Measurement of transepithelial electrical resistance (TER) and paracellular permeability

Cells grown to confluency underwent normoxia or hypoxia for the indicated times. The monolayer TER was measured using an electrovoltohmeter (EVOM; World Precision Instruments, Sarasota, FL, USA). Paracellular permeability was assessed by apical-to-basal transport of a dextran probe (MW3000) conjugated to fluorescein (Invitrogen) as described previously (Yu et al., 2005; Wu et al., 2011).

Immunofluorescent staining of tight junction structures

Cells were exposed to normoxia or hypoxia for 16 hrs, fixed with 4% paraformaldehyde for one hour on ice, and quenched with 50 mM NH4Cl in PBS for 10 min at room temperature. After blocking with 0.1% bovine serum albumin (BSA) in PBS for one hour, monolayers were incubated with a polyclonal rabbit anti-human ZO-1 antibody (1:100, Invitrogen) in a permeabilizing buffer (0.05% saponin, and 0.1% BSA in PBS) for one hour. Cells were then incubated with secondary antibodies of goat anti-rabbit IgG conjugated to Alexa 488 (1:1000, Invitrogen) for one hour in the dark,

and then stained with a Hoechst dye to visualize cell nuclei. The slides were mounted with aqueous mounting media and viewed under a Zeiss fluorescence microscope.

Measurement of cell apoptosis

DNA fragmentation, which is a final stage of apoptosis, was measured using a cell detection ELISA kit (Roche) for oligonucleosome amount as previously described (Yu et al., 2005). The caspse-3 activity assay (Anaspec) was based on spectrophotometric detection of chromophore rhodamine 110 (Rh110) after cleavage from the labeled substrate DEVD- Rh110 according to the manufacturer's instructions (Huang et al., 2011).

RNA extraction and polymerase chain reaction (PCR) for GLUT transcripts

Total RNA was isolated using Trizol reagent (Invitrogen) according to the manufacturer's instructions. For semiquantitative PCR analysis, the RNA (2 μg) was reverse transcribed (RT) with oligo(dT) using RevertAid First Strant cDNA Synthesis kit (Thermo) in 20 μL reaction volume. The RT product corresponding to 0.1 μg of initial RNA was subjected to PCR amplification in a thermal cycler. The specific primer pairs of human GLUTs 1-4 and β-actin and the thermal cycling procedures were described previously *(Noguchi et al., 2000).* The amplification conditions were as

followed: denaturation at 95°C for 30 sec, annealing at 60°C for 30 sec and extension at 72°C for 50 sec in a total of 30 cycles. The PCR products were separated onto 1% agarose gel containing ethidium bromide, and visualized by ultraviolet transillumination.

Quantitative real-time PCR analysis was carried out using an Applied Biosystems 7500 Real-Time PCR system (Applied Biosystems). The PCR reaction mixture consisted of 50 ng of RT product, 10 μL of Power SYBR Green PCR Master Mix (Applied Biosystems) and 500 nM specific primer pairs in a final reaction volume of 20 μL. The specific primer pairs of human GLUT1, GLUT4 and β-actin were described previously *(Matsushita et al., 2012; Torres et al., 2012)*. The PCR conditions were 95 °C for 10 min, followed by 40 cycles of denaturation at 95 °C for 15 sec, and annealing and extension at 56 °C for 1 min. Amplification plots were obtained by using a Sequence Detection Software (Applied Biosystems).

Western blotting for GLUT proteins in human colonic carcinoma cells

Extracted protein samples were subjected to SDS/PAGE (4–13% polyacrylamide) as described *(Huang et al., 2011; Wu et al., 2011)*. Briefly, the resolved proteins were electrotransferred onto PVDF membranes and blocked with 5% (w/v) nonfat dry milk in Tris-buffered saline (TBS) for 1 hr, washed three times with TBS-T (0.1% (v/v)

Tween-20 in TBS), and then incubated with primary antibodies at 4°C overnight. After washing with TBS-T, the membrane was incubated with a secondary antibody for 1 hr and then washed again. The membranes were incubated with chemiluminescent solution (ECL, Millipore) and signal was detected on an UVP AutoChemi system (UVP, Upland). Band density was determined using the software Gel-pro Analyzer 4.0 (Media Cybernetics).

The primary antibodies used for blotting included anti-GLUT1 (1:2000, Millipore), anti-GLUT2 (1:1000, Millipore), anti-GLUT3 (1:1000, Millipore), anti-GLUT4 (1:1000, Millipore), and anti-β-actin (1:10000, Sigma). The secondary antibody used were horseradish peroxidase-conjugated goat anti-rabbit IgG (1:1000, Cell Signaling).

Measurement of intracellular redox enzyme activities

The activities of catalase, superoxide dismutase (SOD), glutathione reductase (GR), or glutathione-S-transferase (GST) were measured in cell lysates using commercial assay kits (Cayman Chemical, MI, USA) following the manufacturer's instructions.

Measurement of intracellular pyruvate, ATP, and lactate contents

Cell lysates were used for the assessment of intracellular pyruvate (Biovision, CA, USA), ATP (Invitrogen) and lactate (Biovision) levels using commercial assay kits. To measure the pyruvate concentration in the cell, pyruvate is served as a substrate

oxidized by pyruvate oxidase via enzyme reaction to generate color and analysis at OD 570 nm by plate reader. The ATP assay is based on requirement of ATP by luciferase for light production, and the luminescence is measured using a luminometer. To quantify lactate content, a chromogenic assay utilizing cellular lactate as a substrate oxidized by lactate dehydrogenase was measured at 450 nm by a plate reader.

Statistical analysis

All values except for bacterial CFU/g were expressed as mean ± SEM and the means were compared by one-way analysis of variance followed by a Student-Newman-Keul test. For the data of BT, pairwise ranking of the median of CFU/g values was conducted using the nonparametric Mann-Whitney *U* test. Significance was established at $P < 0.05$.

Chapter 3 RESULTS

The results of part 1 and part 2 were adopted from Ching-Ying Huang's papers in Laboratory Investigation (Huang et al., 2011) and Cell Death and Disease (Huang et al., 2013).

3.1 Part 1

Mesenteric I/R triggers intestinal epithelial apoptosis that accompanies villous destruction

Compared with non-ischemic tissues in sham controls, rats subjected to mesenteric I/R showed villous blunting and epithelial denudation in the jejunum (Figure. 1A). Mucosal destruction was associated with increased number of TUNEL(+) epithelial cells and enhanced immunoreactivity to cleaved caspase-3 at regions close to the denuded villous tips in intestines of I/R rats (Figure. 1B and 1C). Decreased immunoreactivity of PCNA was found in the intestinal crypts in I/R rats compared to sham controls (Figure. 1D). The severity of mucosal damage caused by I/R was quantified by histopathological scoring (Figure. 1E).

Enteral instillation of the pancaspase inhibitor ZVAD reduced the degree of mucosal injury and epithelial apoptosis caused by I/R (Figure. 1A-C, and 1E). Normal intestinal histology was seen in sham-operated rats enterally administered ZVAD

(Figure. 1A). The mucosal caspase-3 activity was significantly increased after ischemia (Table 1). Luminal pretreatment with ZVAD inhibited both baseline and ischemia-induced mucosal caspase-3 activity (Table 3-1). This parameter was not measured post-reperfusion owing to the marked destruction of the villous structure.

To assess the changes in the tight junctional structure, the level of occludin was evaluated by Western blot. Increased cleavage of occludin was seen in the intestinal mucosa of ischemic intestines compared to that of sham operation (Figure. 2). Pretreatment with ZVAD diminished the level of occludin cleavage caused by ischemic challenge (Figure. 2). Occludin levels were not examined post-reperfusion due to severe epithelial denudation.

Increased intestinal permeability caused by I/R is dependent on epithelial apoptosis

The intestinal permeability changes caused by I/R were first evaluated using an *ex vivo* assay that measured the luminal-to-serosal flux of a macromolecular probe HRP in Ussing chambers (Yu et al., 2003). The transmural HRP flux rate in the intestine of I/R rats was twice that of sham controls. The increase of HRP flux in I/R tissues compared to sham controls was evident at 30-60 and 60-90 minutes after luminal addition of HRP to the chambers (Figure. 3A).

In consideration of the time frame required to detect increased HRP flux and the extracorporeal setting of high oxygen and glucose supply needed to maintain the viability of tissues *ex vivo* — which may produce artificial results of the extent of I/R injury — we also measured gut permeability changes *in vivo* by using ligated loops administered with fluorescein-conjugated dextran (Wang et al., 1998) or a contrast agent gadodiamide for the newly-developed MRI-based assay (Hsiao et al., 2009). A significant increase of the lumen-to-blood passage of FITC-dextran was seen in I/R rats compared to sham controls (Figure. 3B).

The novel MRI-based intestinal permeability assay monitors the portal drainage of an enterally-administered contrast agent (gadodiamide) by quantifying the signals in the liver and kidney as the areas of interest (Hsiao et al., 2009). Representative abdominal images of sham and I/R rats were taken at various time points after the start of reperfusion (Figure. 3C). The signals in liver and kidney in I/R rats were brighter than in sham controls (Figure. 3C). The signal-to-noise ratio (SNR) of the areas of interest was quantified from the MR images (Figure. 3D). The liver SNR values in sham controls was consistently low throughout these time points, whereas in I/R rats the liver signals were significantly elevated over time and remained high up to 60 minutes post-reperfusion (Figure. 3D). The signal intensity in liver was 14 times higher in I/R rats (SNR = 4.97 ± 0.45) than in sham controls (SNR = 0.35 ± 0.07) as early as 5

minutes post-reperfusion (Figure. 3D). The kidney SNR values in I/R rats were significantly higher than that of sham controls within 15 minutes post-reperfusion (Figure. 3D). The plasma gadodiamide concentration was 68 times higher in I/R rats than in sham controls (Figure. 3D).

Pretreatment with intraluminal ZVAD partially decreased the gut permeability rise triggered by I/R, as evidenced by lower fluorescein intensity in plasma samples (Figure. 3B), as well as lower SNR in the liver, kidney, and plasma in I/R+Z rats (Figure. 3C and 3-3D). The gut permeability in sham+Z rats was comparable to that of sham controls (data not shown).

I/R-induced enteric bacterial translocation and mucosal inflammation are diminished by pretreatment with a caspase inhibitor

The bacterial counts in liver tissue in I/R rats were significantly higher than sham controls (Figure. 4A). A similar increase of bacterial CFUs was demonstrated in the spleen upon I/R insult (Figure. 4B). Intraluminal pretreatment with ZVAD abolished the increase in bacterial CFUs in the liver and spleen of I/R rats (Figure. 4A and 4B).

The intestinal MPO activity (Figure. 5) and the mucosal levels of TNFα and MIP-1α (Figure. 6) were higher in ischemic intestines compared to those with sham operation, suggesting activation of inflammatory cells. Enteral instillation of ZVAD

diminished the rise of MPO activity (Figure. 5) and the increase of TNFα and MIP-1α production induced by ischemia (Figure. 6). The inflammatory parameters in sham+Z rats were comparable to those of sham controls (data not shown).

Luminal glucose decreased I/R-induced intestinal pathology

Mucosal pathology and epithelial apoptosis

Enteral instillation of glucose significantly alleviated I/R-induced mucosal injury, whereby the jejunal villi showed better structure and were covered by intact epithelial layers without cell apoptosis, and the crypt regions showed PCNA immunoreactivity (Figure. 1A-D). Normal intestinal histology was seen in sham+G rats (Fig. 1A). Luminal glucose also reduced the increase in mucosal caspase-3 activity caused by intestinal ischemia (Table 1).

Tight junctional integrity and epithelial permeability

The effect of glucose on intestinal barrier function was examined further. Enteral instillation of glucose reduced the level of occludin cleavage in ischemic guts (Figure. 2).

Moreover, the presence of luminal glucose during I/R challenge diminished the lumen-to-blood passage of FITC-dextran (Figure. 3B), as well as the gadodiamide signals and SNR in the liver, kidney, and plasma samples (Figure. 3C and 3D).

Bacterial translocation and mucosal inflammation

The I/R-triggered increase of BT was abolished by luminal glucose. The bacterial counts in liver and spleen were significantly lower in I/R+G rats than in I/R rats (Figure. 4A and 4B). The bacterial counts in sham+G rats were comparable to those of sham controls (data not shown).

The intestinal MPO activity in I/R+G rats was decreased compared with I/R rats (Figure. 5). Reduced mucosal levels of TNFα and MIP-1α were seen in ischemic intestines instilled with enteric glucose (Figure. 6A and 6B). The intestinal inflammatory parameters in sham+G rats were comparable to those of sham controls (data not shown).

Phloridzin blockage of SGLT1 sugar uptake nullifies glucose protection in a dose-dependent manner

To verify the role of SGLT1 in the protective mechanism, pharmacological inhibitors of specific transporters were instilled into the ligated sac in the presence of glucose and the gut permeability changes were measured by MRI-based assay. We found that luminal pretreatment with phloridzin (a specific SGLT1 inhibitor; 0.5-2.5 mM) dose-dependently increased the liver SNR values of I/R+G rats to levels comparable to those of I/R rats (Figure. 7A). Phloridzin (2.5 mM) also inhibited the

glucose-mediated reduction of BT (Figure. 7B). On the other hand, pretreatment with phloretin (an inhibitor of GLUT2; 2.5 mM) did not diminish the protective effect of glucose on gut permeability (Figure. 7A) and BT (Figure. 7B). Moreover, apical expression of SGLT1 was confirmed in the jejunal epithelium in sham controls (Figure. 7C). A lack of SGLT1 staining accompanied the epithelial sloughing seen in I/R rat intestines; the presence of luminal glucose abolished this decrease (Figure. 7C).

PI3K/Akt signaling are involved in the glucose-mediated cell survival mechanism

To verify the involvement of PI3K/Akt signals in the glucose-mediated cytoprotective mechanism, I/R+G rats were administered LY294002 (LY) or wortmannin (W), which partially eliminated the glucose protection against I/R-induced cell apoptosis and villous destruction (Figure. 8A) as well as permeability rise (Figure. 8B).

The activation status of Akt in gut mucosa was investigated by measuring the kinase reaction of immunoprecipitated phospho-Akt to phosphorylate exogenous GSK3 in an *in vitro* assay. Decreased Akt activity in the intestinal mucosa of I/R rats was evidenced by the lower levels of phosphorylated GSK3 in I/R samples than in sham groups (Figure. 9A). Enteral instillation of glucose increased the mucosal Akt activity in both sham and I/R tissues (Figure. 9A). The GSK3 phosphorylation levels in samples

from I/R+G+LY rats was lower than I/R+G rats (Figure. 9B), indicating that specific inhibition of PI3K by LY294002 partly diminished the glucose-mediated activation of Akt. Furthermore, immunofluorescent staining demonstrated the cytosolic expression of Akt in jejunal epithelial cells in sham controls (Figure. 9C-a). Enteral instillation of glucose induced the translocation of cytosolic Akt to the brush border and subcellular organelles of enterocytes in sham+G rats (Figure. 9C-b). The loss of Akt expression was correlated with the sloughing of intestinal epithelium in I/R rats (Figure. 9C-c), in which these changes were attenuated by the addition of luminal glucose (Figure. 9C-d). The phenomenon of Akt translocation to the brush border and to subcellular organelles in epithelial cells was also seen in I/R+G rats (Figure. 9C-d).

The phosphorylation levels of Akt and downstream signals such as IκB, mTOR, Bad, and FoxO1/3a in the mucosa of ischemic tissues were investigated by Western blot. These parameters were not measured post-reperfusion due to severe mucosal denudation. A significant decrease in phosphorylated Akt level was seen in ischemic tissues compared to sham controls (Figure. 10A). Increased phosphorylation of Akt was seen after enteral instillation of glucose in both sham and ischemic tissues (Figure. 10A). Recent data indicate a link between Akt and IκBα/NFκB signals in promotion of cell survival and resistance to apoptosis in enterocytes (Dan et al., 2008; Bai et al., 2009). On the other hand, IκBα/NFκB signals also play key roles in proinflammatory cytokine

production in monocytes/macrophages and intestinal epithelial cells (Funda et al., 2001; Suzuki et al., 2003; Selvaraj et al., 2005; Murphy et al., 2010). Our data showed that the mucosal level of phospho-IκBα was significantly increased after ischemic challenge compared to sham controls (Figure. 10B). Enteral instillation of glucose diminished the increase of IκBα phosphorylation caused by ischemia (Figure. 10B). Lastly, the phosphorylation of Akt correlated with the phosphorylation of mTOR, Bad, and FoxO1/3a in ischemic tissues with glucose instillation (Figure. 10C).

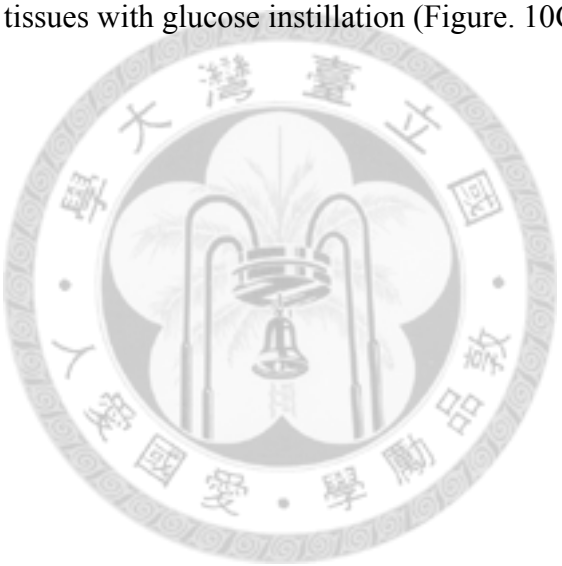

3.2 Part 2

Hypoxic challenge triggers RIP-dependent necroptosis in human colorectal carcinoma cells

Human colorectal carcinoma Caco-2 cells were exposed to normoxia (Nx) or hypoxia (Hx) in glucose-free media (Φ) for various time points, and a time-dependent increase of LDH leakage was observed in Hx+Φ but not Nx+Φ cells (Figure 12A). Live images revealed cytosolic vacuolation, widening intercellular space, and cell detachment in a timely order following hypoxic challenge, whereas no morphological change was observed in normoxic counterparts (Figure 12B). No sign of apoptosis was found after hypoxic challenge as evidenced by the lack of oligonucleosome formation and caspase-3 activation (Figure 13). Similar results of hypoxia-induced cell necrosis were seen in another human colorectal tumor cell line HT29 (Figure 14A and B).

The mitochondrial transmembrane potential was determined by using a cationic JC-1 dye. Exposure to hypoxia resulted in a transient increase and then decline in red fluorescence intensity (the aggregated form of JC-1) followed by a display of green fluorescence (the monomer form of JC-1) in the cytoplasm at later time points (Figure 12C). Quantification results indicated that the ratios of J-aggregate/monomer in cells after 8- and 24-hr hypoxia were 221.1 ± 49.0% and 20.5 ± 2.8%, respectively, of that of

the normoxic controls (Figure 12D), suggesting that hypoxia caused a transient hyperpolarization and a final collapse of mitochondrial transmembrane potential.

Furthermore, plasma membrane disintegration paralleled with loss of tight junctions in hypoxic cells, evidenced by reduction of transepithelial electrical resistance (TER), increase of apical-to-basolateral dextran flux, and structural disruption of zonula occluden-1 (ZO-1) (Figure 12E-G).

Pretreatment with necrostatin-1 (a specific RIP1 inhibitor) and gene silencing of RIP1 reduced the level of LDH leakage caused by hypoxic challenge (Figure 15A and 3-2B). A ~50% knock down of RIP1 protein by siRNA was confirmed by Western blots (Figure 15B). Using immunoprecipitation and 32P kinase assays, formation of RIP1/3 complex and phosphorylation of RIP1 were found in Hx+Φ but not Nx+Φ cells (Figure 16A), indicating the activation of RIP1/3 signaling. The hypoxia-induced morphological damage and cell detachment were also inhibited by necrostatin-1 (Figure 15C). However, the mitochondrial transmembrane potential change was not reverted by necrostatin-1 (Figure 15D), suggesting that RIP1 activation may not be upstream of mitochondrial dysfunction. In hypoxic cells treated with necrostain-1, a transient increase in red fluorescence was seen after 8 hrs followed by a switch to green fluorescence after 24 hrs (Figure 15D), of which the quantification results of JC-1 staining were 277.2 ± 25.2% and 40.2 ± 13.6%, compared to normoxic controls with

necrostain-1 at respective time points.

Glucose uptake abolishes hypoxia-induced RIP signaling and necroptosis

Administration of glucose (25 mM) reduced the RIP1/3 complex formation and phosphorylation (Figure 16A) and decreased LDH leakage in hypoxic cells in a dose-dependent manner (Figure 16B). Non-metabolizable sugar analogs (i.e. 3-OMG and mannitol) or glutamate did not reduce the LDH activity (Figure 17). Moreover, glucose addition also ablated hypoxia-induced morphological damages (data not shown), mitochondrial transmembrane potential damage (Figure 16C), and tight junctional disruption (Figure 16D-F). Addition of glucose did not modify the apoptotic levels in hypoxic cells (data not shown).

To confirm that cells still perceive hypoxic stress after glucose addition, activation of HIF1α and hypoxia-targeted genes were examined. Nuclear translocation of HIF1α (Figure 18A) correlated with increased expression of GLUT-1 and -4 at the transcriptional and translational levels in hypoxic cells given glucose (Figure 18B-D). The experiment was not carried out on hypoxic cells in glucose-free media due to cell necrosis (i.e. plasma membrane disintegration and release of cellular contents). Moreover, similar results of glucose-mediated death resistance, HIF1α activation, and GLUT upregulation were also seen in HT29 cells under hypoxic stress (Figure. 19A, C,

D).

Anaerobic glycolytic metabolism is involved in anti-necrotic resistance to hypoxia stress

To verify the metabolic process that is involved in death resistance, cells were pretreated with iodoacetate (IA, a glycolytic inhibitor to GPD) and UK5399 (UK, a MPC inhibitor) prior to hypoxic challenge in the presence of glucose. Blockade of glucose-mediated resistance was noted in cells pretreated with IA, whereas no inhibitory effect was seen with UK (Figure 20A), suggesting that glycolytic products unrelated to TCA cycles were involved in anti-necrotic mechanisms. For hypoxic cells in glucose-free media, IA and UK had no effect on LDH activity (data not shown).

The intracellular ATP, pyruvate, lactate contents were next quantified to examine the bioenergetic status of cells. A significant reduction of intracellular ATP and pyruvate levels were seen in hypoxic cells compared to their normoxic controls in glucose-free media (Figure 20B and C), whereas comparable lactate production was noted between the two groups (Figure 20D). Addition of glucose partially prevented the drop of ATP and pyruvate caused by hypoxia, and significantly increased the lactate contents (Figure 20B-D). The effect of IA was confirmed by lower levels of ATP, pyruvate, and lactate production compared to those given glucose without inhibitors in both normoxic and

hypoxic conditions (Figure 20B-D). In contrast, UK had no effect on these parameters (Figure 20B-D).

Pyruvate is involved in death resistance through mitochondrial superoxide scavenging without restoration of cellular energy

The specific role of pyruvate in the mechanisms of death resistance was examined by replacing glucose with cell-permeable ethyl pyruvate derivative in hypoxic cells. Addition of pyruvate derivative significantly reduced the LDH leakage, RIP1/3 complex formation, and morphological damage in hypoxic cells (Figure 21A-C). However, the ATP levels in cells given pyruvate were comparable to those without supplementation (Figure 21D). Presence of pyruvate neither altered cellular ATP contents nor suppressed dextran flux in hypoxic cells (Figure 21E), indicating that death resistance by pyruvate was uncoupled with ATP production and energy-dependent processes (e.g. tight junctional restoration). Unlike glucose, pyruvate did not suppress hypoxia-induced mitochondrial transmembrane potential changes (Figure 21F). These results suggest that pyruvate confers resistance to necroptosis through an alternative, energy-independent mechanism.

Generation of mitochondria-derived oxidative free radicals has been implicated in the cell necrotic pathways triggered by cytotoxic agents (Declercq et al., 2009; Zhang et

al., 2009), and we sought to examine its role in hypoxic necrosis. Increased mean fluorescence of MitoSox (an indicator of mitochondrial superoxide production) was observed in hypoxic cells compared to normoxic controls in glucose-free media (Figure 22A). Decreasing the mitochondrial superoxide levels with butylated hydroxyanisole (BHA, a free radical scavenger) and apocynin (an inhibitor to nicotinamide adenine dinucleotide phosphate (NADPH) oxidase) (Figure 22A) led to partial inhibition of LDH leakage in hypoxic cells (Figure 22B). Moreover, pretreatment with BHA also diminished the RIP1/3 complex formation (Figure 22C). These results indicate that ROS production which is upstream of RIP signaling is involved in hypoxia-induced necroptotic pathways.

The modulatory effect of glucose and pyruvate on free radical levels was next addressed. Addition of glucose decreased hypoxia-induced mitochondrial ROS levels (Figure 22D), but did not alter the redox activities of catalase, superoxide dismutase, glutathione reductase, or glutathione-S-transferase (Figure 23), suggesting a non-enzymatic scavenging mechanism. The glucose-mediated reduction of mitochondrial ROS may be inhibited by pretreatment with IA but not UK (Figure 22D). Lastly, replacing glucose with cell-permeable pyruvate derivative also significantly suppressed the mitochondrial ROS levels in hypoxic cells (Figure 22D). Similar results of pyruvate-mediated resistance were seen in HT29 cells under hypoxic stress (Figure

19B, E).

Chapter 4 DISCUSSION

The first part of our results demonstrate that enterocytic apoptosis is in part responsible for triggering intestinal barrier dysfunction upon I/R challenge, and glucose uptake mediated by SGLT1 attenuated the loss of intestinal barrier function partly via anti-apoptotic PI3K/Akt signaling (Figure. 11).

The histological findings suggest that mesenteric I/R triggers epithelial apoptosis that accompanies villous disintegration and decreased crypt cell proliferation. Changes in intestinal permeability in I/R rats were demonstrated by the transmural HRP flux rate *ex vivo* and by the lumen-to-blood passage of enterally-administered FD4 and gadodiamide *in vivo*. The increase of epithelial permeability paralleled the augmentation of BT in I/R intestines, indicating gut barrier damage. These pathological changes were attenuated by enteral instillation of ZVAD, providing direct evidence that epithelial apoptosis is in part responsible for triggering intestinal barrier damage and bacterial influx. This study is thus the first to demonstrate that modification of epithelial caspase activity reduces intestinal permeability and BT in animals. We also showed that pretreatment with ZVAD diminished the increase of MPO activity and the production of TNFα and MIP-1α in ischemic intestines, suggesting that epithelial apoptosis and barrier dysfunction preceded mucosal inflammation.

The intestinal permeability was evaluated using *ex vivo* and *in vivo* assays. A twofold increase of the transmural HRP flux was observed in the intestinal tissues in I/R rats compared with sham controls. However, the increased HRP flux was only evident at 30-60 and 60-90 minutes after the addition of the probe to Ussing chambers; the delayed observation and the extracorporeal, oxygenated setting may produce artificial results of the extent of I/R injury. In light of these technical limitations, we also evaluated gut permeability *in vivo* by measuring the luminal-to-blood passage of enterally administered FD4 or gadodiamide during the reperfusion period. The plasma level of FD4 was four times higher in I/R rats than in sham controls, indicating compromised intestinal barrier function after ischemic challenge. A novel MRI-based assay developed previously from our laboratory was used to detect the real-time permeability changes *in vivo*. This more sensitive assay showed a five- to tenfold increase of SNR in liver and kidney in ischemic rats at the early phase (<15 minutes) of reperfusion, supporting the hypothesis that it is an acute break of the epithelial barrier that leads to augmented portal drainage of luminal probes. The kidney SNR peaked at 15 minutes post-reperfusion and declined afterwards, which was likely due to the high concentration of gadodiamide in the renal medulla and calyces leading to a greater T2 shortening effect than T1 shortening effect. These results are in agreement with others showing increased gut permeability upon I/R challenge (Sun et al., 1998; Khanna et al.,

2001). In comparison to the HRP flux assay and the fluorescence intensity test, this MRI-based method is fast and sensitive, and allows us to rapidly detect changes in gut permeability and provides a means for further studies of targeted pharmacological intervention.

Physiological cytoprotective mechanisms contributing to resistance against apoptosis include upregulation of glucose transporters (e.g. SGLT1, GLUT1, and GLUT4) and maintenance of high intracellular glucose concentration (Sun et al., 1994; Hall et al., 2001; Russo et al., 2004; Yu et al., 2005; Yu et al., 2006; Wofford et al., 2008; Yu et al., 2008). The phenomenon of glucose protection has been documented in a number of cell types, including neurons, leukocytes, myocardiocytes, and vascular smooth muscle cells (Sun et al., 1994; Hall et al., 2001; Russo et al., 2004; Wofford et al., 2008). Previous *in vitro* studies utilizing human intestinal epithelial Caco-2 cells have also demonstrated that SGLT1 glucose uptake inhibits cell apoptosis and barrier impairment caused by bacterial and parasitic products (Yu et al., 2005; Yu et al., 2006; Yu et al., 2008). Based on our finding that epithelial apoptosis is partly responsible for intestinal barrier dysfunction upon I/R challenge, we sought to investigate the use of glucose supplementation to correct excessive cell death and to improve gut barrier integrity. In I/R rats, glucose uptake mediated by the phloridzin-sensitive SGLT1 protected the intestinal epithelium from apoptosis and attenuated the increase in

permeability and BT, leading to diminished inflammatory responses. Taken together with previous studies (Yu et al., 2005; Yu et al., 2006; Yu et al., 2008), our finding suggests that SGLT1-mediated cytoprotection may operate under a number of metabolic and microbial stress conditions.

The signal transduction pathways responsible for promoting cell survival were also investigated. Membrane translocation and increased phosphorylation of Akt in villous epithelial cells were paralleled by enhanced Akt kinase activity in the gut mucosa following glucose uptake by SGLT1. This finding is consistent with previous studies showing that Akt is a downstream step of a signaling pathway induced by Na^+-glucose cotransport (Zhao et al., 2004; Shiue et al., 2005), which triggered the activation of Na^+-H^+ exchanger (NHE). Our pharmacological blockade studies with LY294002 and wortmannin confirmed that PI3K/Akt activation is involved in the glucose-mediated protection against epithelial apoptosis, mucosal pathology and gut barrier damage induced by I/R. Previous reports documented that PI3K/Akt signaling inhibits cell apoptosis by phosphorylating Bad, either directly or indirectly via mTOR (Chang et al., 2003; LoPiccolo et al., 2008). A number of other downstream targets of Akt, such as IκBα/NFκBα, FoxO1/3a and GSK3, are also involved in promoting cell survival and cell cycle progression (Liang et al., 2003; Urbich et al., 2005; Dan et al., 2008; Bai et al., 2009). We showed here that SGLT1 glucose uptake induced the phosphorylation of Akt

and downstream targets such as mTOR, Bad and FoxO1/3a in intestinal mucosa. These results provide an explanation of the anti-apoptotic effects of enteral glucose, which may contribute to cytoprotective mechanisms in intestinal I/R. It is noteworthy that recent evidence points to an unanticipated role of Bad in linking pathways of glucose metabolism and cell apoptosis (Danial et al., 2003; Danial, 2008). Danial *et al.* demonstrated that Bad resides in a mitochondrial complex with glucokinase and participates in mitochondrial respiration in response to glucose (Danial et al., 2003; Danial, 2008). The phosphorylation status of Bad is associated with glucokinase activity; glucose deprivation results in dephosphorylation of Bad and Bad-dependent cell death (Danial et al., 2003; Danial, 2008). These findings highlight the role that mitochondrial Bad plays in coordinating glucose metabolism and the apoptotic machinery. Whether the phosphorylation status of mitochondrial Bad affects the mode of glucose metabolism in ischemic intestines requires further investigation.

Recent reports indicated that the IκBα/NFκB pathway is involved in anti-apoptotic events in intestinal epithelial cells against various pathogenic stimuli (Potoka et al., 2000; Egan et al., 2004; Nenci et al., 2007). However, our results demonstrated that instillation of enteric glucose decreased the levels of phosphorylated IκBα in ischemic guts. Despite links between Akt and IκBα/NFκB pathways in the mechanism of cell survival (Chang et al., 2003; Dan et al., 2008; Bai et al., 2009), the IκBα/NFκB pathway

is not involved in the glucose-mediated anti-apoptotic signaling in intestinal epithelium. The upregulation of phospho-IκBα may be partly responsible for proinflammatory cytokine production after ischemic challenge. Overall, we demonstrated that SGLT1 glucose uptake in intestinal epithelial cells activated anti-apoptotic pathways that involved PI3K/Akt signaling and increased phosphorylation of mTOR, Bad and FoxO1/3a.

Accumulating data supports the notion that SGLT1 orchestrates a number of fundamental cellular processes besides its canonical absorptive function. Previous reports showed that activation of SGLT1 induced the recruitment of GLUT2 to the brush border membrane for diffusive glucose transport via a PKCβ-dependent pathway (Kellett et al., 2000; Kellett, 2001). Others documented that cotransport of Na^+ with glucose triggered the activation of Akt and phosphorylation of cytoskeleton-associated ezrin, leading to recruitment of NHE to apical membrane that facilitated absorption of sodium and hydrogen in intestines (Zhao et al., 2004; Shiue et al., 2005). A recent study by Palazzo *et al*. demonstrated that activation of SGLT1 suppressed bacterial LPS-induced NF κ B signaling in intestinal epithelial cells, and suggested that SGLT1 plays a novel immunomodulatory role (Palazzo et al., 2008). Moreover, oral ingestion but not intraperitoneal administration of glucose attenuated proinflammatory cytokine production and protected endotoxemic mice from lethal septic shock (Palazzo et al.,

2008). Clinically, oral rehydration therapy that targets SGLT1 to drive passive diffusion of water is a widely-used supportive therapy for diarrheal patients. Early enteral nutrition (EN) is advocated for patients with multiple pathologies for its known benefit in lowering the risk of septic complications compared to parenteral supplementation. One area that has gained much attention in nutrition therapy nowadays is preoperative oral carbohydrate loading (CHO) (Fearon et al., 2005; Martindale et al., 2006). This novel concept involves giving patients an isotonic carbohydrate solution at midnight the day before surgery and 2-3 hours preoperatively, in contrast to the general routine of overnight fasting before surgery. Patients given CHO showed reduced postoperative insulin resistance and shorter hospital stay after colorectal resection (Soop et al., 2004). The advantage of early EN and CHO may also involve SGLT1-mediated nutritive and non-nutritive functions.

The second part of our study demonstrates a novel mechanism through which glycolytic pyruvate confers resistance to RIP-dependent necroptosis in hypoxic colorectal carcinoma via mitochondrial superoxide scavenging. Despite long-standing observation of cell necrosis in the hypoxic core of colorectal tumors, there is an apparent lack of knowledge on its molecular mechanisms. In our study, we demonstrated that oxygen and glucose deprivation induced RIP-1/3 signaling and morphological necrotic features, i.e. rupture of plasma membrane, 8 to 24 hours after

the onset of challenge in colorectal carcinoma cells. Recent studies from other laboratories have also showed necroptosis in intestinal epithelial cells in models of chronic intestinal inflammation in gene-deficient mice (Gunther et al., 2011; Welz et al., 2011). Although there is no data on the timing of necrotic death caused by hypoxic stress in normal human epithelial cells, rapid villous necrosis in jejunum and colon was found in rats after 60 minutes of hemorrhagic shock or 40 minutes of mesenteric ischemia (Chang et al., 2005; Higa et al., 2007), showing that normal cells are more sensitive to oxygen and nutrient deprivation compared to cancer cells. It is noteworthy that normoxic controls in glucose-free media displayed no sign of necroptosis, indicating that glucose deprivation alone did not trigger necrotic death.

Mitochondrial dysfunctions and free radical generation have also been implicated in the necrotic process caused by cytotoxic agents.(Goossens et al., 1995; Temkin et al., 2006; Zhang et al., 2009). The transient mitochondrial hyperpolarization observed in our study may reflect a temporal reversal of electron transport chain ATP synthase activity due to a decline in intracellular oxygen, leading to adverse proton pumping against the electrochemical gradient to intermembranous spaces. Moreover, the final mitochondrial potential collapse correlated well with organelle swelling at later time points (16-24 hrs) of hypoxia. Interestingly, we identified high levels of mitochondrial superoxide production prior to plasma membrane disintegration in hypoxic colonic

carcinoma cells. This seemingly paradoxical situation of ROS emission in hypoxia has also been previously documented in cardiomyocytes after infarction (Becker et al., 1999; Camara et al., 2007). The generation of mitochondrial ROS has been suggested to be caused by electron leak to oxygen in the respiratory chain complexes whereby low levels of oxygen remain inside cells at the early stage of hypoxic challenge (Turrens, 2003). By using antioxidants, we demonstrated that mitochondria-derived superoxide plays a critical role in hypoxia-induced necrotic mechanisms and is upstream of RIP signals.

We further showed that GLUT-dependent glucose uptake and glycolytic metabolism inhibits hypoxia-induced RIP signaling and necrotic features in colorectal cancer cells. Several studies have implicated that glycolytically generated ATP may restore energy supply in cancer cells and act as a key factor for glucose-mediated death resistance against hypoxia and genotoxic agents (Xu et al., 2005; Zhou et al., 2012). Recent data in activated macrophages and B lymphocytes have demonstrated that glycolytic ATP promotes cell survival via maintenance of transmembrane potential of defective mitochondria that are unable to generate ATP (Dufort et al., 2007; Garedew et al., 2010). Here, we focused on the role of glycolytic pyruvate, and examined if cell-permeable derivative may lead to anti-necrotic effects. We demonstrated that hypoxia-induced necroptosis (i.e. LDH leakage, RIP activation, and morphological

damage) was reverted by pyruvate, however, the resistance was uncoupled with restoration of cellular energy and mitochondrial potential. Another line of evidence showed that glucose addition reduced the mitochondrial ROS levels but did not alter the redox enzyme activity. The aforementioned data indicate that a non-enzymatic free radical scavenging mechanism, such as those reported with pyruvate, may contribute to death resistance. Indeed, our results showed that supplementation of pyruvate significantly reduced the mitochondrial superoxide levels in hypoxic cells in an ATP-independent manner. It is noteworthy that glucose-mediated recovery of mitochondrial transmembrane potential in hypoxic cells is not dependent on pyruvate but may rely on ATP. Taken together, glycolytic metabolism may promote hypoxic cell survival by a two-fold mechanism including scavenging of mitochondrial superoxide by pyruvate and maintenance of mitochondrial potential by ATP.

We confirmed that presence of glucose during hypoxic challenge did not ablate oxygen deprivation stress as evidenced by the nuclear translocation of HIF1α. The HIF1-targeted upregulation of GLUTs led to enhanced glucose uptake and glycolytic metabolism, serving as a positive cycle to promote cell survival. Normal human small intestinal epithelial cells express SGLT1 on apical membrane and GLUT2 on basolateral membrane for luminal-to-serosal flux of dietary glucose absorption (Yu et al., 2005; Yu et al., 2008). In contrast to normal colonocytes, human colorectal carcinoma specimens

abnormally display SGLT1 and GLUT isoforms 1-4 on the apical membrane or cytoplasm of tumor cells (Godoy et al., 2006; Guo et al., 2011; de Wit et al., 2012). Previous studies have indicated that transcriptional regulation of GLUT1 is mediated by HIF1 binding to a nucleotide sequence corresponding to a hypoxia-responsive element in promoter regions of GLUT1 gene, following oxygen deprivation (Ouiddir et al., 1999; Hayashi et al., 2004).

Other than glucose transporters (GLUT1 and GLUT3), a large number of genes encoding for glycolytic enzymes, angiogenic growth factors, cell survival and proliferative signals, and prolyl hydroxylases (PHD) are also upregulated by HIF1 (Denko, 2008; Chiacchiera et al., 2009; Marin-Hernandez et al., 2009). In our study, a transient drop of GLUTs expression was observed after 16 hrs but recovered after 24 hrs of hypoxia. The temporary reduction of GLUTs expression may be due to the regulatory loop of HIF1α/PHD. Under normoxic conditions, PHD-mediated hydroxylation of proline residues on HIF1α permits its ubiquitination followed by proteosomal degradation. Hypoxia sensing downregulates PHD activity and thus, stabilizes HIF1α levels, leading to its nuclear translocation and downstream transcription of target genes (Jaakkola et al., 2001; Kondo et al., 2006). Paradoxically, PHDs are themselves target genes of HIF1 transcription, indicating a negative feedback mechanism *(Marxsen et al., 2004; Stiehl et al., 2006).* In addition, HIF1α degrades within 8-12 hrs without *de novo*

synthesis (Millonig et al., 2009). Therefore, we speculate that the fluctuation of GLUTs expression after the onset of hypoxia may reflect the HIF1α/PHD loop. Experiments to address the temporal relationship, cellular distribution, and pathophysiological significance of various isoforms of glucose transporters by HIF1 in colonic carcinoma are currently under progress.

Angiogenic pathways and mediators have been extensively studied as potential anti-cancer drugs for several decades. In some cases, patients fail to respond to antiangiogenic agents or simply develop drug resistance. Tumors may display invasive metastatic transition in response to the increasing hypoxic microenvironment by cancer treatment (Zeng et al., 2010; Rapisarda et al., 2012). Here, our data show a critical role of glycolytic pyruvate in death resistance and underscore site-specific glucose transporters and metabolic pathways as potential candidates for the development of novel cancer killing strategies. The resistance to antiangiogesis or hypoxic stress may be overcome by combinational strategies with glucose- or pyruvate-targeted therapy. In summary, the second part of the studies demonstrated glycolytic metabolism inhibits hypoxia-induced RIP-dependentnecroptosis in colonic cancer cells by suppression of mitochondrial ROS (Figure 24).

Chapter 5 TABLE AND FIGURES

5.1 Table

Table 1 Caspase-3 activity in the jejunal mucosa in rats.

	Sham	I	I+Z	I+G
Caspase-3 activity (RFU/min/mg protein)	9800 ± 1381	15114 ± 362 *	94 ± 7 *#	11888 ± 891 #

Rats were subjected to sham operation (Sham) or ischemic (I) challenge for 20 minutes with or without enteral instillation of a pancaspase inhibitor ZVAD (Z) and glucose (G). *$P < 0.05$ *vs*. Sham, #$P < 0.05$ *vs*. I. (n = 6 / group)

5.2 Figures

Figure 1

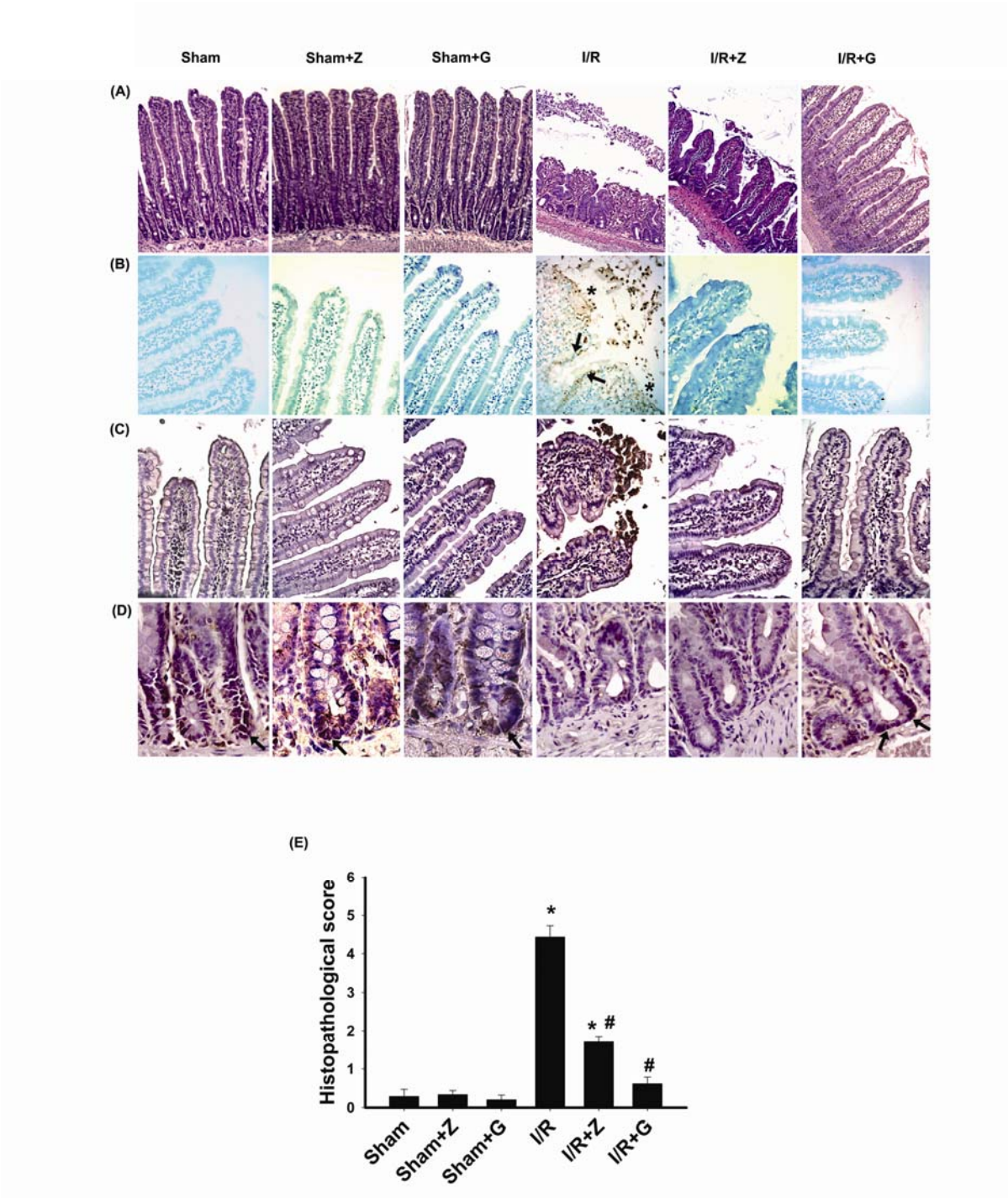

Figure 1 Mesenteric I/R triggers enterocytic apoptosis that accompanies villous destruction. The jejunal tissues of sham-operated and I/R rats were processed for **(A)** H&E staining, **(B)** TUNEL assay, and immunostaining of **(C)** cleaved caspase-3, and **(D)** PCNA. Magnification: 200× in (A); Magnification: 400× in (B-D). **(A)** In comparison to non-ischemic tissues in sham controls, mucosal injury including villous blunting and epithelial denudation were observed in I/R rats. Enteral instillation of 120 μM ZVAD (Z) or 25 mM glucose (G) alleviated I/R-induced morphologic injury (labeled I/R+Z and I/R+G, respectively). Normal mucosal histology was seen in sham+Z and sham+G rats. **(B)** Enterocytes with increased TUNEL(+) reaction were noted in regions close to the denuded villous apex after mesenteric I/R. TUNEL(+) epithelial cells (arrows) and villous denudation (asterisks) were observed in the intestines of I/R rats. Enteral instillation of ZVAD or glucose decreased I/R-induced epithelial apoptosis. **(C)** Increased immunoreactivity to cleaved caspase-3 was seen at villous tips in I/R rats compared to sham controls. No staining was observed in intestinal tissues in sham+Z, sham+G, I/R+Z and I/R+G rats. **(D)** Immunoreactivity to PCNA (arrows) was detected in intestinal crypts in sham, sham+Z, and sham+G rats, No staining was seen in intestinal tissues in I/R rats. Enteral instillation of glucose attenuated the I/R-induced decrease of PCNA immunoreactivity, whereas ZVAD had no effect. **(E)** Histopathological scores in jejunal tissues of each group of rats. $*P<0.05$ *vs.* sham, $^{\#}P<0.05$ *vs.* I/R. (n = 6–8 / group)

Figure 2

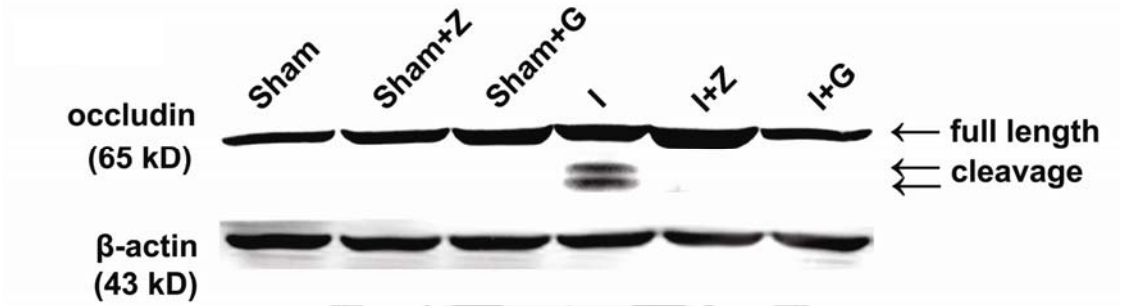

Figure 2 Increased cleavage of tight junctional occludin after ischemic challenge is alleviated by enteral instillation of ZVAD or glucose. Western blot images of occludin in jejunal mucosa of rats subjected to sham operation (Sham) and ischemic (I) challenge with or without enteral instillation of ZVAD (Z) or glucose (G). Representative images from 4 separate experiments. (n = 4 / group)

Figure 3

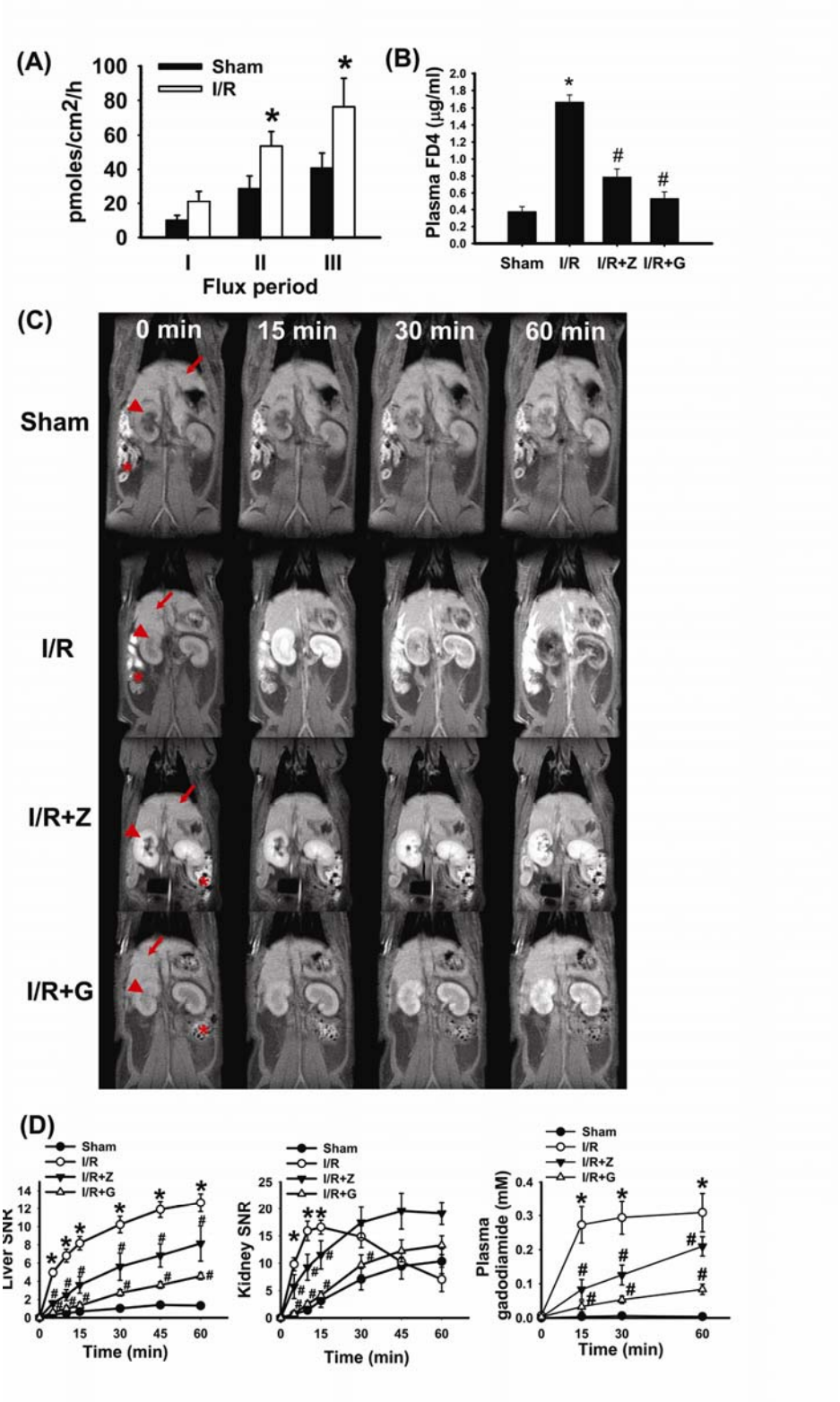
(A)
Sham
I/R
pmoles/cm2/h
Flux period
I
II
III
(B)
Plasma FD4 (μg/ml)
Sham
I/R
I/R+Z
I/R+G
(C)
0 min
15 min
30 min
60 min
Sham
I/R
I/R+Z
I/R+G
(D)
Liver SNR
Kidney SNR
Plasma gadodiamide (mM)
Time (min)

Figure 3 I/R-triggered increase of epithelial permeability is ameliorated by enteral instillation of ZVAD or glucose. (A) Increased mucosal-to-serosal flux of HRP was seen in I/R rats compared to sham controls. HRP in serosal buffer was measured by kinetic enzymatic assay at 0-30 (I), 30-60 (II) and 60-90 (III) minutes after addition of HRP to the luminal buffer. **P* < 0.05 *vs.* sham. **(B)** The 4-kDa FITC dextran (FD4) concentration in plasma sample collected from sham, I/R, I/R+Z and I/R+G rats at 60 min post-reperfusion. A significant increase of the lumen-to-blood passage of FD4 was seen in I/R rats compared to sham controls, which was decreased by instillation of ZVAD or glucose. **(C)** Abdominal images of sham, I/R, I/R+Z and I/R+G rats were taken at 0, 15, 30, and 60 min post-reperfusion. The arrow, arrowhead, and asterisk indicate the location of the liver, kidney, and ligated jejunal sac, respectively. In all panels, "0 min" indicates images taken before luminal gadodiamide was instilled into the jejunal sacs. **(D)** SNRs in the liver, kidney, and plasma samples were higher in I/R rats than in sham controls. The I/R-induced increase of gut permeability was ameliorated by enteral instillation of ZVAD or glucose. **P* < 0.05 *vs*. sham; $^{\#}P$ < 0.05 *vs*. I/R. (n = 5–6 / group)

Figure 4

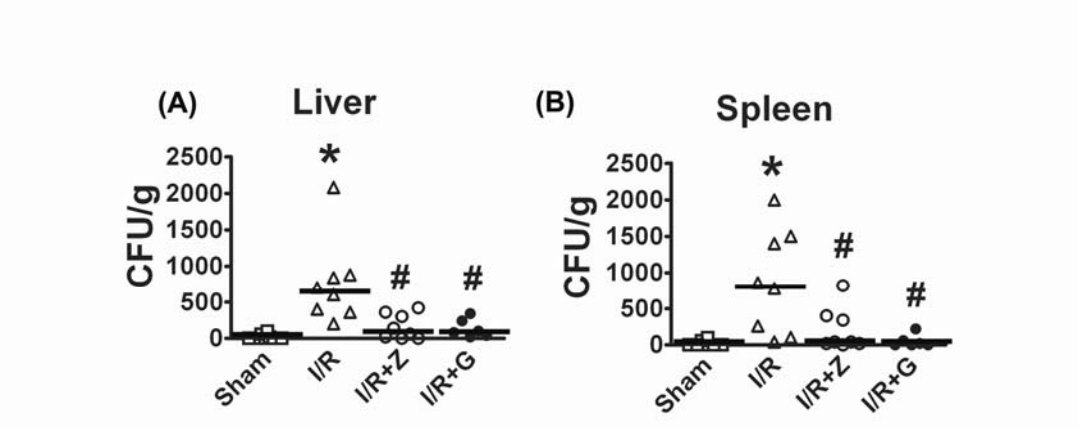

Figure 4 I/R-induced enteric bacterial translocation is diminished by ZVAD or glucose. Numbers of bacterial CFUs in liver **(A)** and spleen **(B)** of sham, I/R, I/R+Z, and I/R+G rats were normalized to tissue weight. Each data point in the figure represents the value from one animal. The median values of bacterial counts (shown as bars) were significantly higher in I/R rats than in sham controls. The increase in bacterial counts caused by I/R was reduced by luminal instillation of ZVAD or glucose. $^{*}P < 0.05$ *vs*. sham; $^{\#}P < 0.05$ *vs*. I/R. (n = 6–8 / group)

Figure 5

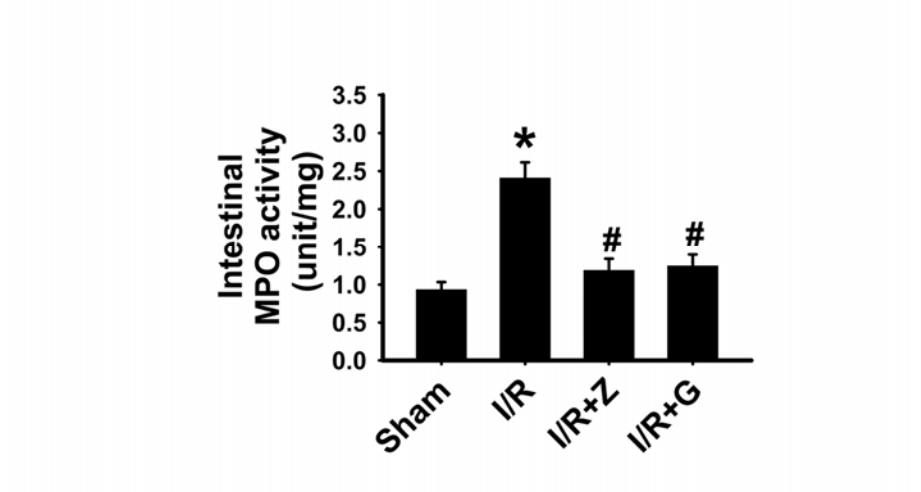

Figure 5 Increased MPO activity caused by I/R is reduced by enteral instillation of ZVAD or glucose. The jejunal tissues of sham, I/R, I/R+Z and I/R+G rats were processed for the measurement of MPO activity (see Methods). One unit of MPO activity was defined as the quantity of enzyme degrading 1 μmol of H_2O_2 per minute. *$P < 0.05$ *vs*. sham; $^{\#}P < 0.05$ *vs*. I/R. (n = 6–8 / group)

Figure 6

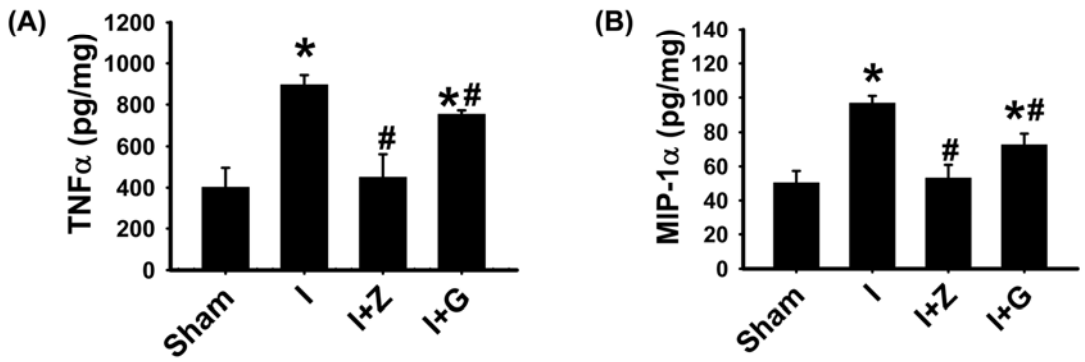

Figure 6 Ischemic challenge augments the production of proinflammatory cytokines in gut mucosa. **(A)** Mucosal levels of TNFα, which increased after ischemic challenge, were attenuated by luminal instillation of ZVAD or glucose. **(B)** The increase of mucosal MIP-1α levels induced by ischemic challenge was ameliorated by ZVAD or glucose. $^{*}P < 0.05$ *vs*. sham; $^{\#}P < 0.05$ *vs*. I. (n = 6 / group)

Figure 7

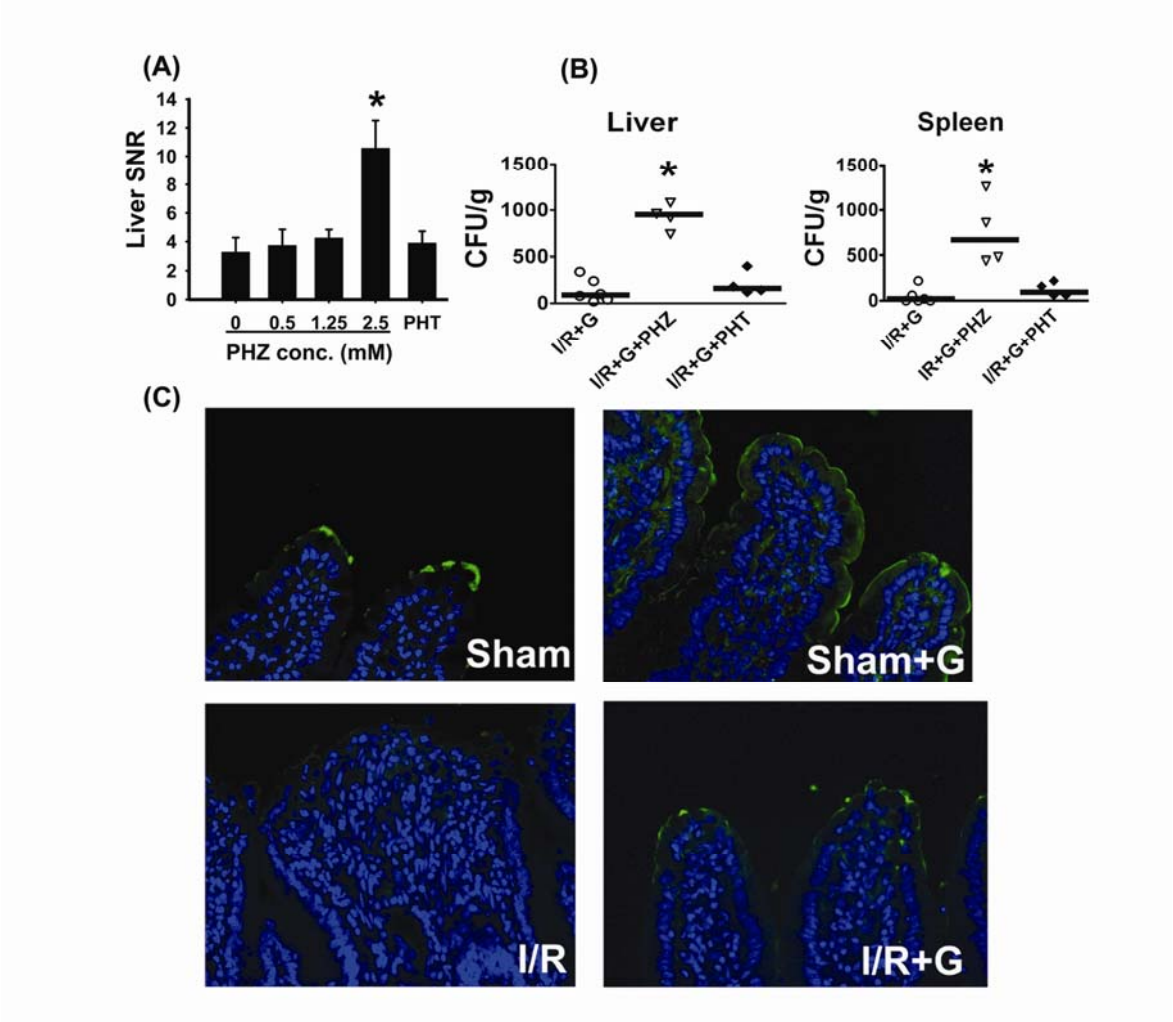

Figure 7 Blockage of phloridzin-sensitive SGLT1 inhibits the glucose protection against I/R-increased epithelial permeability and bacterial translocation. (A) Administration of phloridzin (PHZ) increased the liver SNR in I/R+G rats to a comparable level to I/R rats in a dose-dependent manner. The liver SNR values were acquired at 60 minutes post-reperfusion. Phloretin (PHT) had no effect on the liver SNR values in I/R+G rats. * $P < 0.05$ *vs*. 0 mM phloridzin. **(B)** Glucose-mediated reduction of BT to liver and spleen was abolished by phloridzin (PHZ; 2.5 mM), but not phloretin (PHT; 2.5 mM). The bar represents the median of bacterial counts in each group. * $P < 0.05$ *vs*. I/R+G. **(C)** Immunofluorescent staining demonstrated the apical expression of SGLT1 (green color) on jejunal villi of sham, sham+G, and I/R+G rats. Lack of SGLT1 staining was correlated with epithelial sloughing in the intestine in I/R rats. The cell nuclei are stained blue. (n = 4-6 / group)

Figure 8

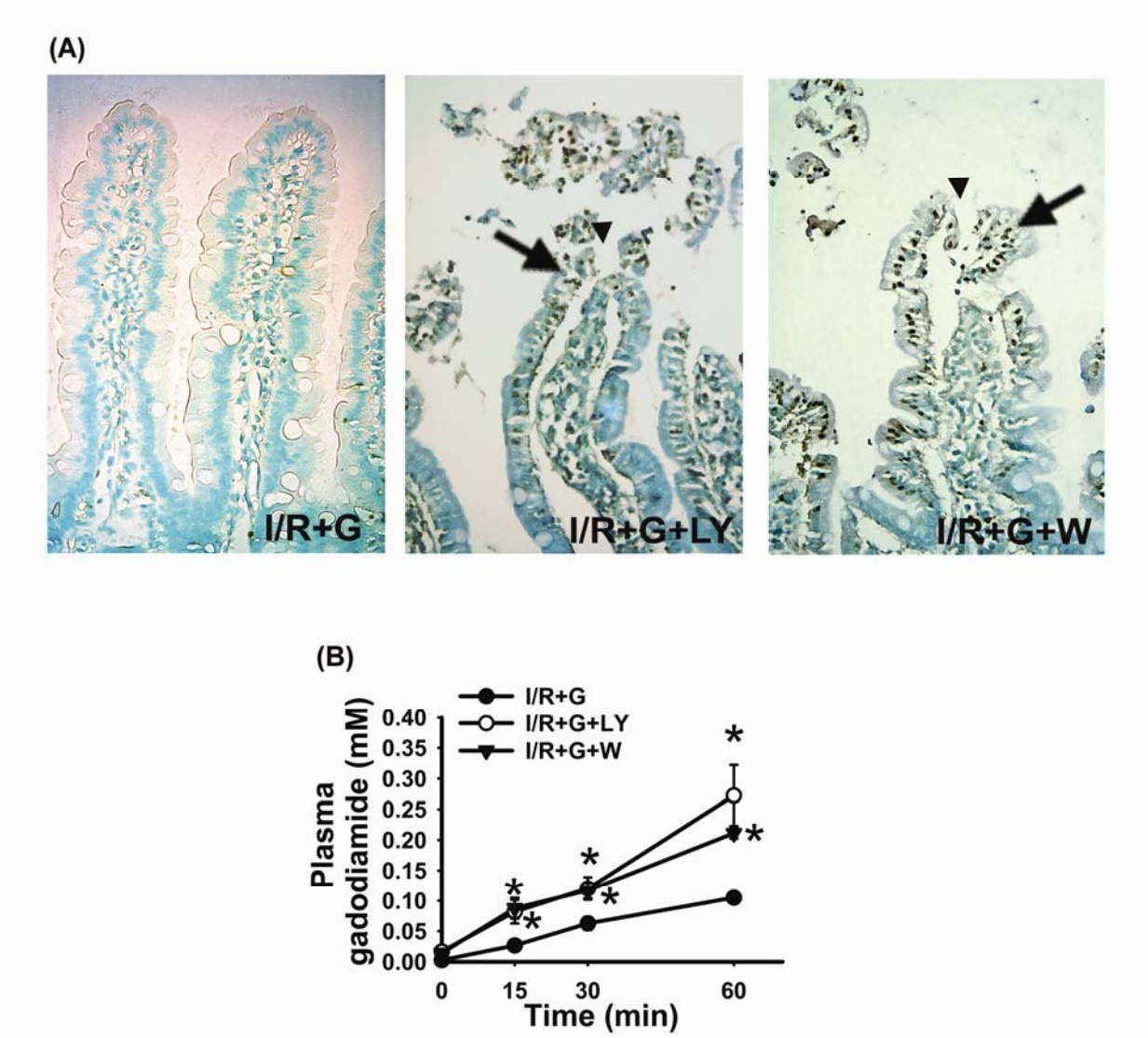

Figure 8 Anti-apoptotic PI3K signaling is involved in the mechanism of glucose protection against I/R-induced intestinal permeability rise. (A) Inhibition of PI3K by LY294002 (LY) or wortmannin (W) blocked the glucose rescue from cell apoptosis caused by I/R. TUNEL(+) epithelial cells (arrows) and disruption of epithelial continuity (arrowheads) were noted in I/R+G+LY and I/R+G+W rats. Magnification: 400×. **(B)** The plasma gadodiamide concentrations in I/R+G+LY and I/R+G+W rats were higher than that of I/R+G rats, indicating that PI3K inhibitors partially diminished the glucose protection against I/R-induced increase of epithelial permeability. **P* < 0.05 *vs*. I/R+G. (n = 6 / group)

Figure 9

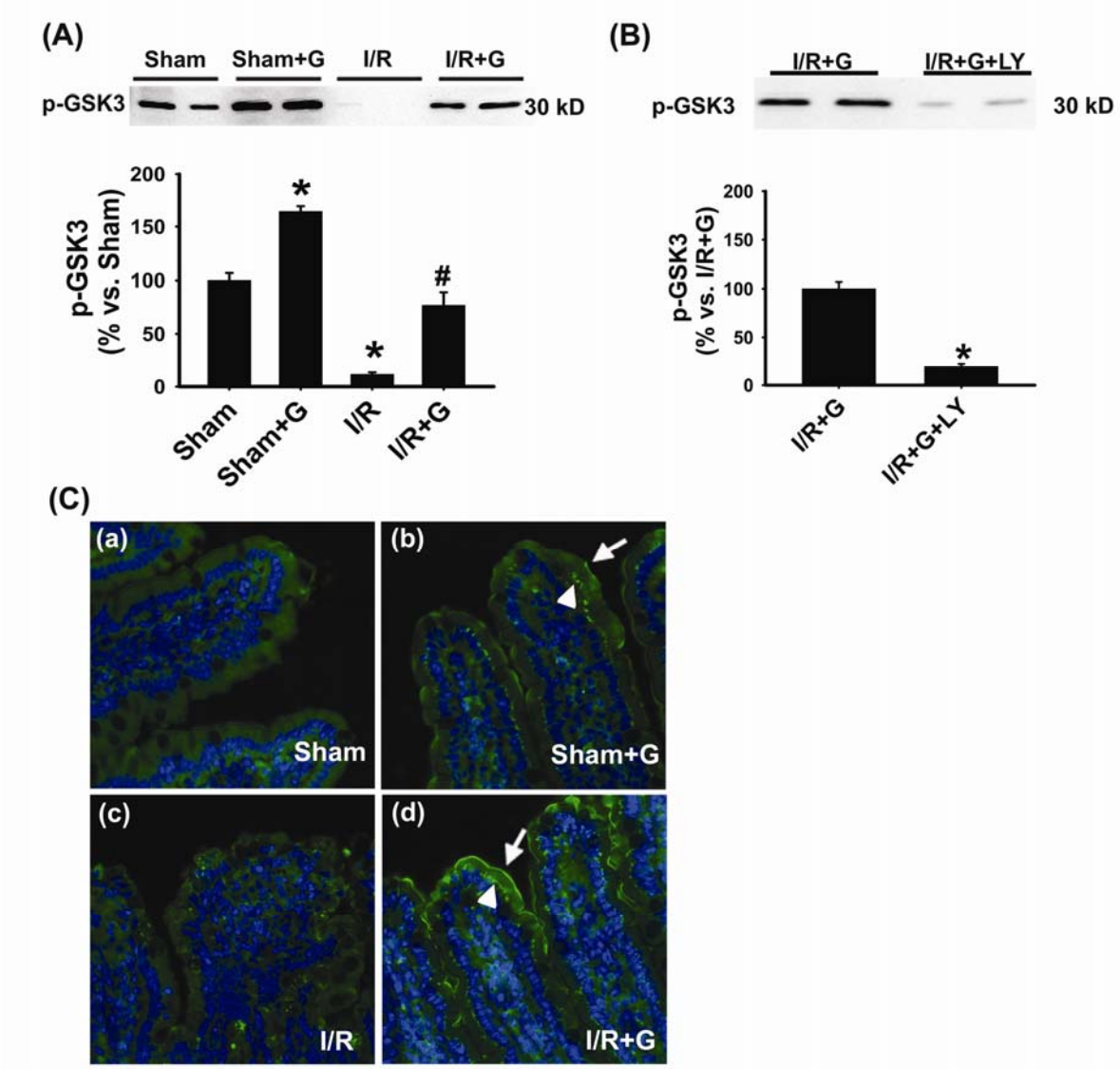

Figure 9 I/R-decreased mucosal Akt activity is inhibited by enteral instillation of glucose. Mucosal lysates from rat jejunal tissues were collected for the measurement of Akt activity. Phospho-Akt protein was immunoprecipitated from the mucosal lysates by anti-phospho-Akt antibody, and exogenous GSK3 served as a substrate for Akt kinase reaction *in vitro*. The level of phospho-GSK3 was examined by Western blot. **(A)** Decreased Akt activity was seen in the intestinal mucosa of I/R rats compared to sham controls. Luminal glucose increased the mucosal Akt activity in both sham and I/R rats. **(B)** Administration of a PI3K inhibitor LY294002 (LY) decreased the mucosal Akt activity in I/R+G rats. **P* < 0.05 *vs*. sham; $^{\#}P < 0.05$ *vs*. I/R. (n = 6 / group) **(C)** Representative images of jejunal tissues stained for Akt (green color); cell nuclei are shown in blue. **(a)** Expression of cytosolic Akt was found in jejunal epithelial cells in sham controls. **(b)** Staining of Akt was noticed on brush border (arrows) and subcellular organelles (arrowheads) in villous epithelial cells in sham+G rats. **(c)** Loss of Akt staining was correlated with epithelial sloughing in I/R rats. **(d)** Histological improvement and staining of Akt on brush border (arrows) and subcellular organelles (arrowheads) in enterocytes were seen in I/R+G rats.

Figure 10

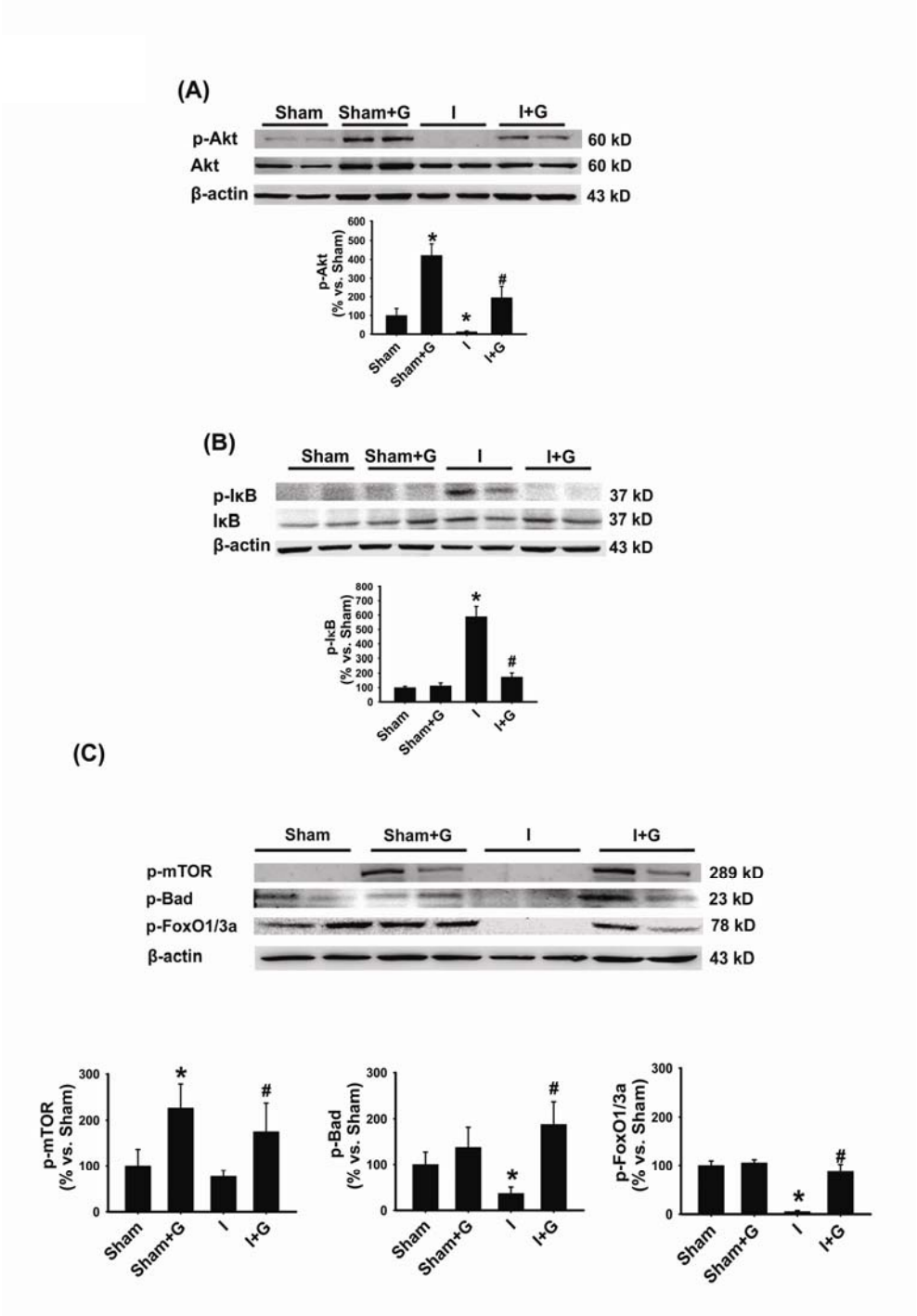

Figure 10 Enteral instillation of glucose induced the phosphorylation of Akt and downstream targets such as mTOR, Bad and FoxO1/3a but not IκBα in ischemic intestines. Western blot showing the levels of phosphorylated Akt, IκBα, mTOR, Bad and FoxO1/3a in jejunal mucosa of sham and ischemic rats after enteral instillation of glucose. Blots from 3 independent experiments were quantified by densitometry. **(A)** Decreased levels of phosphorylated Akt were seen in ischemic tissues compared to sham controls. Luminal glucose increased the phosphorylation of Akt in both sham and ischemic tissues. **(B)** Ischemic challenge augmented the phosphorylation levels of IκBα, which was decreased by glucose. **(C)** Luminal glucose increased the levels of phosphorylated mTOR, Bad and FoxO1/3a in jejunal mucosa in ischemic rats. **P* < 0.05 *vs*. sham; $^{\#}P$ < 0.05 *vs*. I. (n = 6 / group)

Figure 11

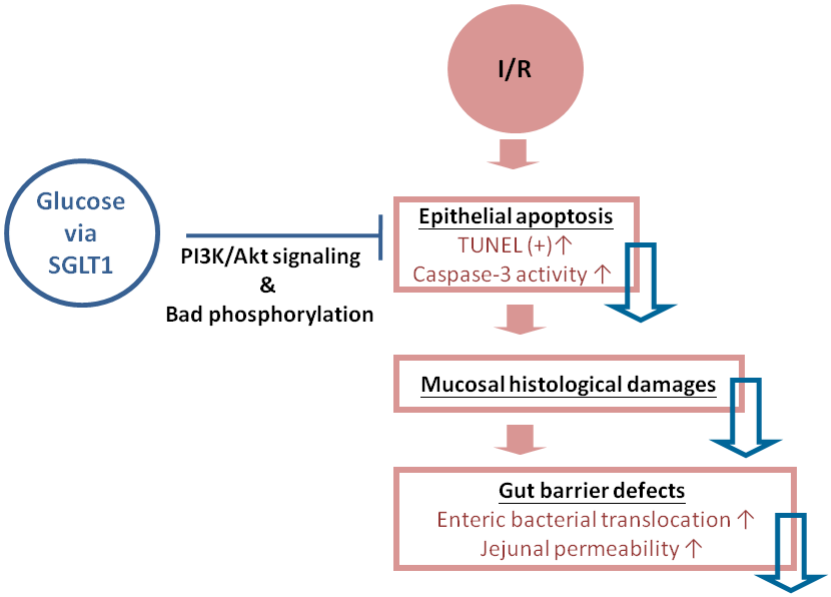

Figure 11 Schema of SGLT1-mediated anti-apoptotic PI3K/Akt signaling pathway attenuated I/R-induced epithelial apoptosis, mucosal damages and barrier defects.

Figure 12

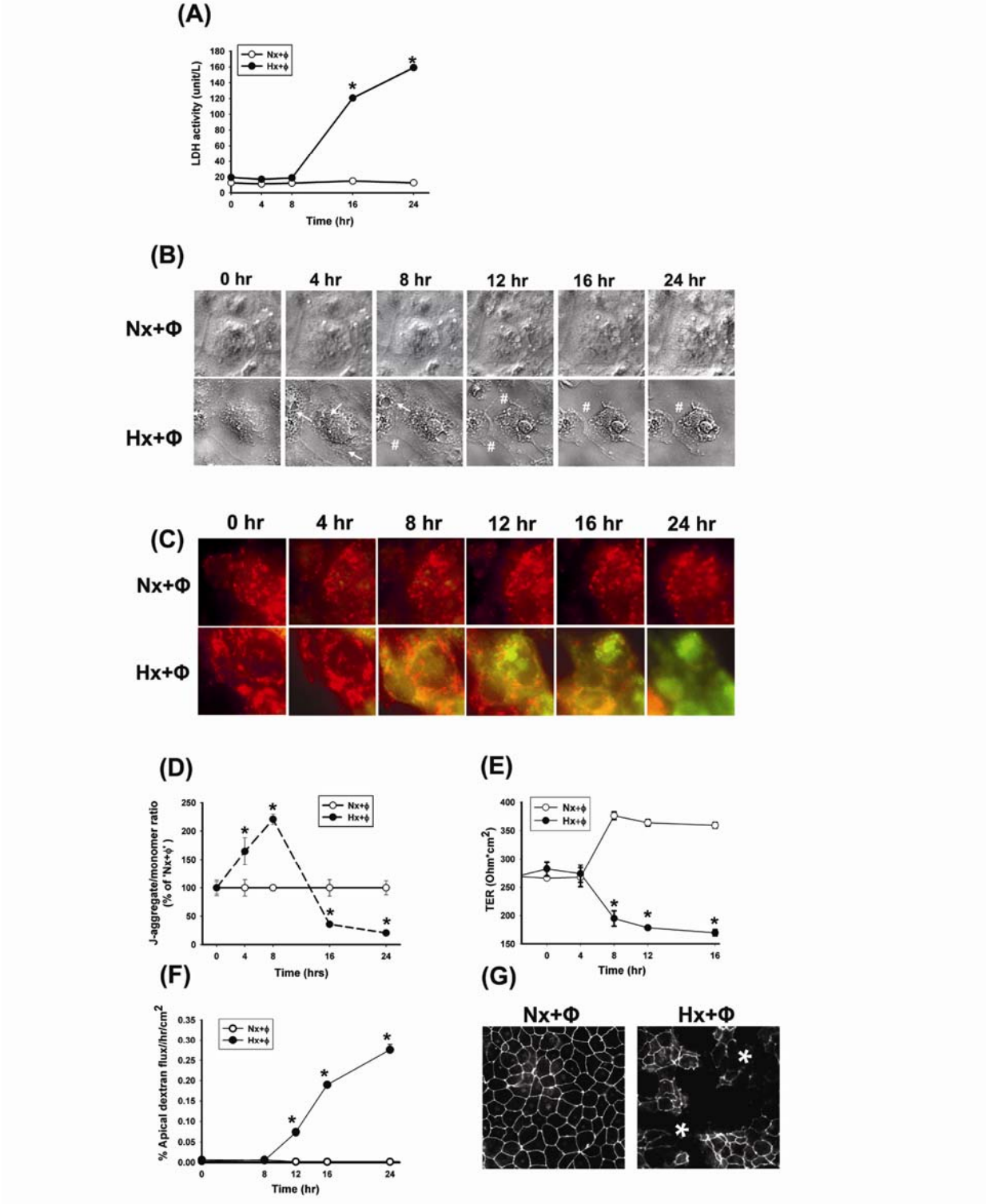
(A)
LDH activity (unit/L)
Nx+ϕ
Hx+ϕ
Time (hr)
(B)
0 hr
4 hr
8 hr
12 hr
16 hr
24 hr
Nx+Φ
Hx+Φ
(C)
(D)
J-aggregate/monomer ratio (% of 'Nx+ϕ')
Time (hrs)
(E)
TER (Ohm*cm2)
(F)
% Apical dextran flux/hr/cm2
(G)

Figure 12 Necrotic death was triggered by hypoxic challenge in human colonic carcinoma cells. (A) Caco-2 cells were exposed to normoxia (Nx) or hypoxia (Hx) in glucose-free media (Φ) for various time points. Increased LDH activity was found in the cell media of Hx+Φ, but not Nx+Φ cells, in a time-dependent manner. **P*<0.05 *vs*. Nx+Φ (n=6/group). **(B)** Representative time-lapse images showing morphological changes in Hx+Φ cells for 24 hrs. Cytosolic vacuolation (→) and cell detachment (#) were noted in Hx+Φ cells. **(C)** Representative time-lapse images showing temporal alterations of mitochondrial transmembrane potential in Hx+Φ, but not Nx+Φ cells. The aggregated form of JC-1 (J-aggregate; red fluorescence) accumulated in functional mitochondria in normoxic cells throughout each time point. In hypoxic cells, a transient increase in red fluorescence intensity was seen after 4-8 hrs followed by a decline at later time points (16-24 hrs) associated with an increase in green fluorescence (the monomer form of JC-1; J-monomer) in the cytoplasm. **(D)** The ratio of J-aggregate to monomer was quantified in Nx+Φ and Hx+Φ cells at various time points. In contrast to normoxic cells, hypoxic challenge induces transient hyperpolarization and a final collapse of the mitochondrial transmembrane potential. **P*<0.05 *vs*. Nx+Φ at individual time points. (n=8/group) **(E)** Hypoxic challenge decreased the transepithelial resistance (TER) of cells compared to normoxic conditions. Data are presented as the absolute TER value at various time points. **P*<0.05 *vs*. Nx+Φ. (n=6/group) **(F)** Hypoxic cells displayed heightened apical-to-basolateral flux of dextran probe in a time-dependent manner. **P*<0.05 *vs*. Nx+Φ. (n=6/group) **(G)** Representative images of tight junction ZO-1 staining in cells exposed to normoxia and hypoxia for 16 hrs. Tight junction disruption and cell detachment (asterisks) were observed in hypoxic cells. (n=6/group)

Figure 13

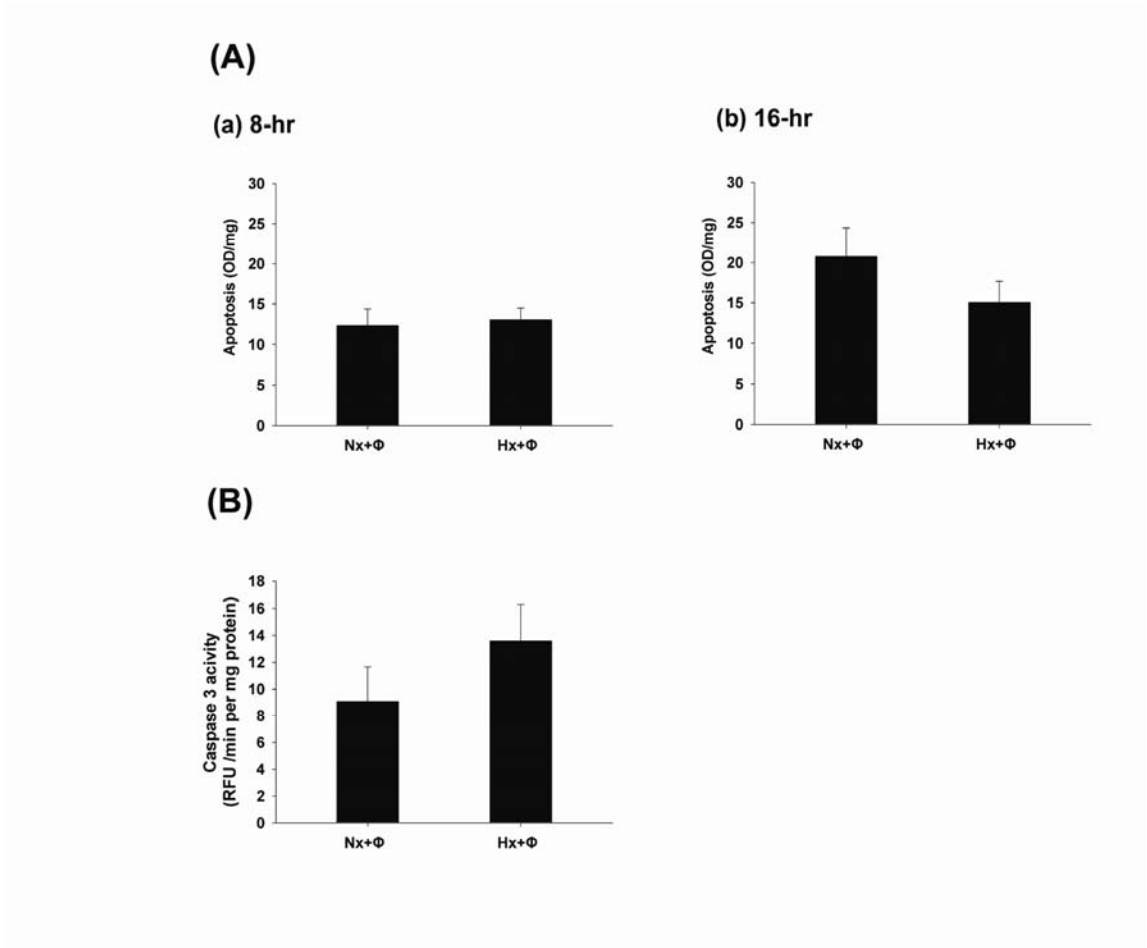

Figure 13 No sign of cell apoptosis was seen after hypoxic challenge. Caco-2 cells were exposed to normoxia (Nx) or hypoxia (Hx) in glucose-free media (Φ) for various time points. **(A)** No increase in oligonucleosome formation (an indicator of DNA fragmentation) was seen in cells exposed to hypoxia in glucose-free media for ***(a)*** 8 hrs and ***(b)*** 16 hrs. **(B)** The caspase-3 activity levels were comparable between hypoxic and normoxic cells at the 8-hr time point. (n=6/group)

Figure 14

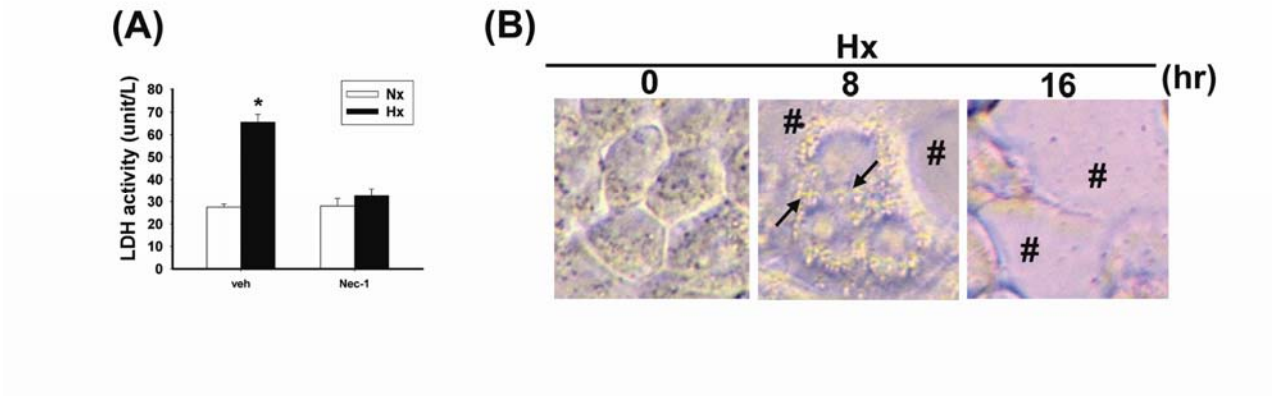

Figure 14 Hypoxic challenge induced LDH leakage and plasma membrane disruption in human colonic carcinoma HT29 cells. (A) HT29 cells were exposed to normoxia (Nx) or hypoxia (Hx) in glucose-free media (Φ) for 16 hrs. Pretreatment with necrostatin-1 (a specific RIP1 inhibitor) decreased the hypoxia-induced LDH leakage. **P*<0.05 *vs*. Nx. (n=6/group). **(B)** Representative photoimages of cells hypoxia exposed for 0, 8, and 16 hrs. Cytosolic vacuolation (→) and cell detachment (#) were noted in Hx+Φ cells. (n=6/group).

Figure 15

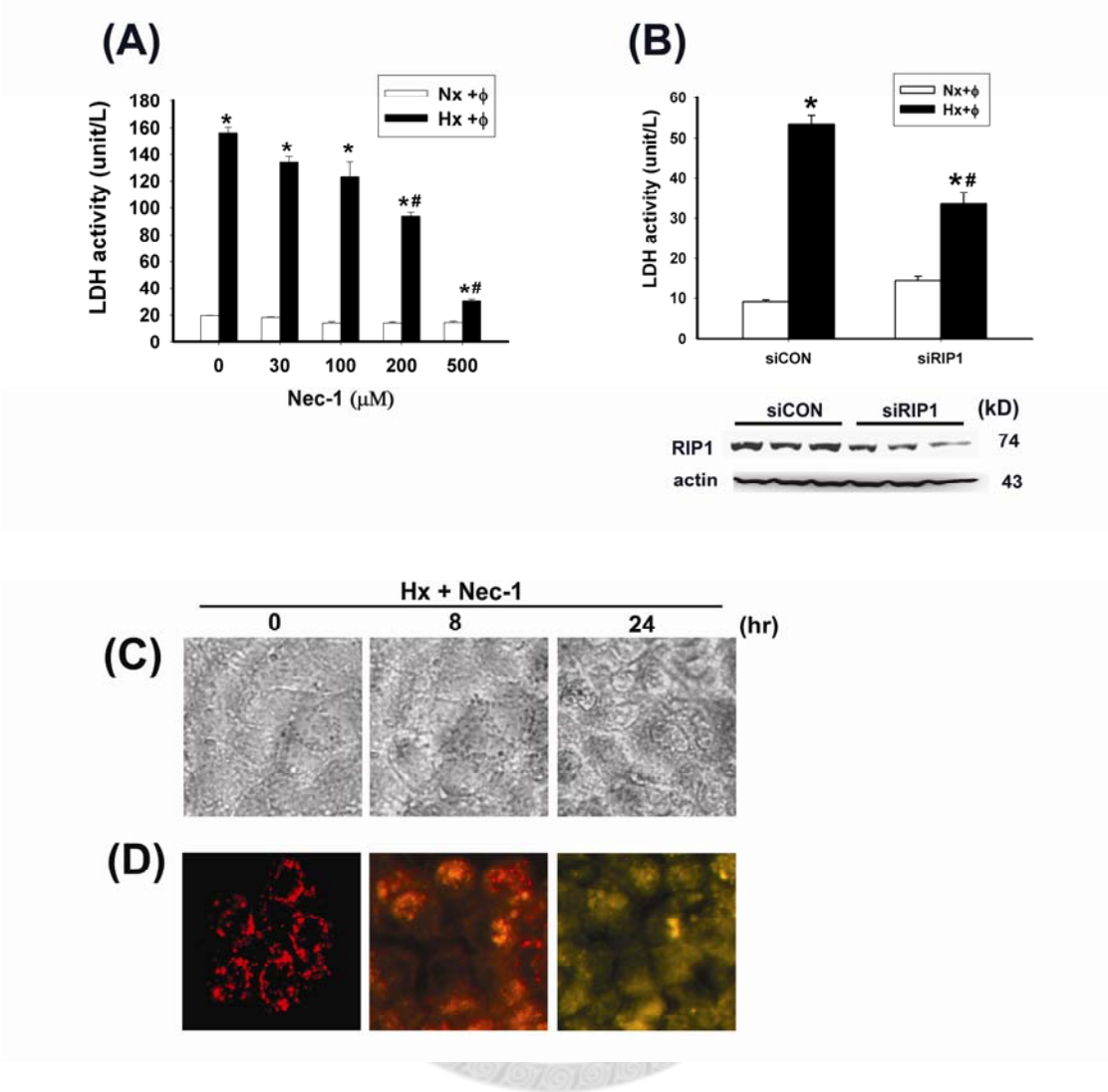

Figure 15 Hypoxia-induced necrotic cell death is dependent on RIP signaling pathways. (A) Pretreatment with necrostatin-1 (a specific RIP1 inhibitor) decreased the hypoxia-induced LDH leakage in a dose-dependent manner. **P*<0.05 *vs*. respective Nx+Φ groups; $^{\#}P$<0.05 *vs*. '0 mM' in Hx+Φ cells. (n=6/group) **(B)** Knockdown of RIP1 by siRNA reduced LDH leakage in hypoxic cells. No effect was seen by negative control (CON) siRNA. Knockdown efficiency of transfected cells was confirmed by Western blots. **P*<0.05 *vs*. respective Nx+Φ groups. $^{\#}P$<0.05 *vs*. CON. (n=3/group) **(C)** Representative images showing that necrostatin-1 inhibited morphological damage and cell detachment caused by 8-hr and 24-hr hypoxia. **(D)** Representative images showing transient mitochondrial hyperpolarization (an increase in red fluorescence intensity after 8 hrs) and a final collapse of transmembrane potential (an increase in green fluorescence intensity after 24 hrs) in hypoxic cells treated with necrostatin-1. The results suggest that RIP1 may not be upstream of mitochondrial dysfunctions. (n=4/group)

Figure 16

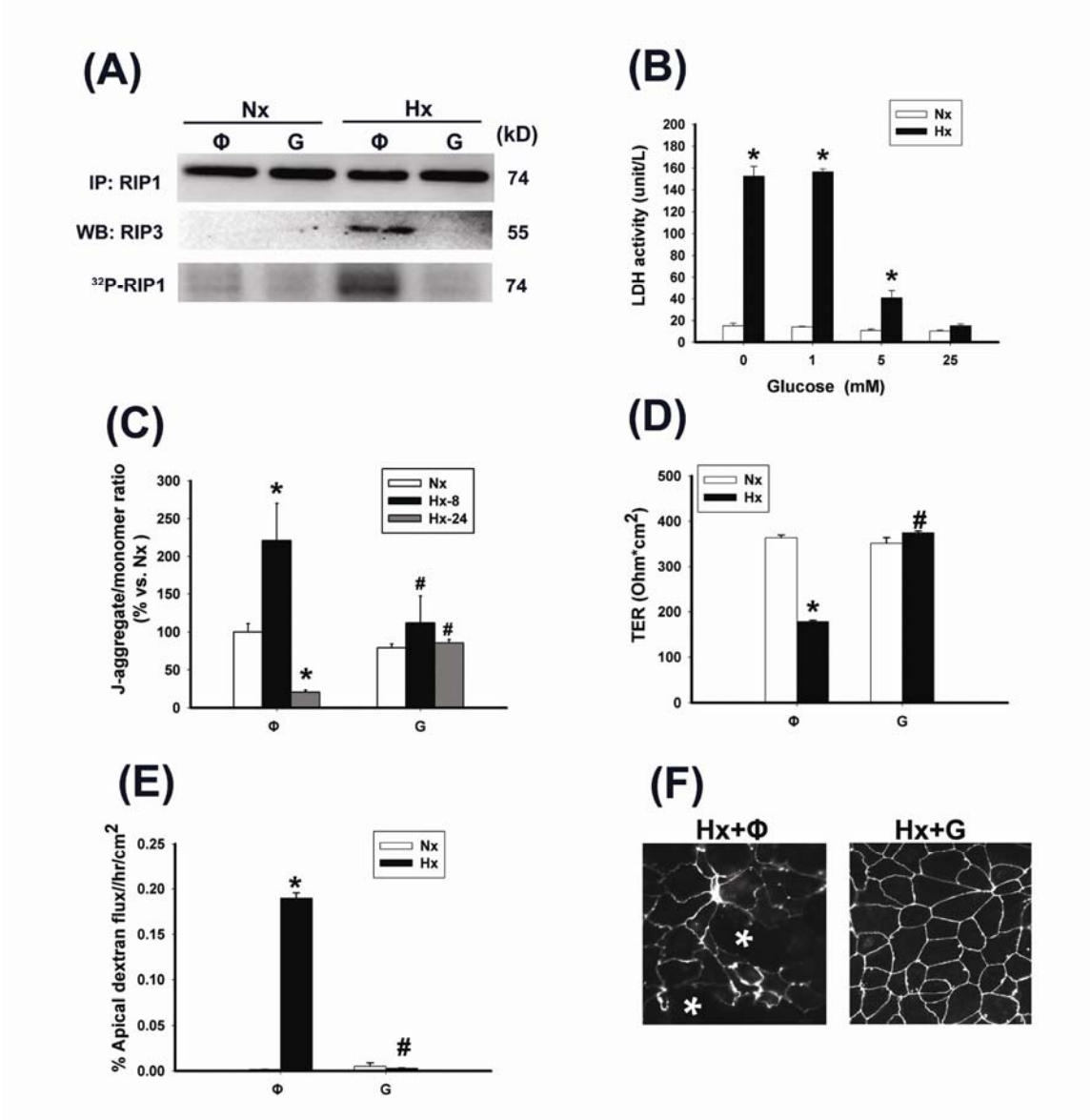

Figure 16 Supplementation of glucose prevented hypoxia-induced necropoptosis in colonic cancer cells. Cells exposed to normoxia (Nx) and hypoxia (Hx) were given glucose (0 or 25 mM) to evaluate death resistance. **(A)** Immunoprecipitation blots showing the formation of RIP1-RIP3 complex and phosphorylation of RIP1 in hypoxic cells without supplementation (labeled as 'Φ'). No sign of RIP signaling was seen in hypoxic cells added 25 mM of glucose (labeled as 'G'), and normoxic counterparts with or without glucose. The experiments were repeated twice and similar results were obtained. (n=3/group). **(B)** The hypoxia-induced LDH leakage was decreased by glucose in a dose-dependent manner. **(C)** The changes in mitochondrial transmembrane potential caused by hypoxic challenge were inhibited by glucose addition. **(D)** The TER drop caused by hypoxia was reversed in cells treated with glucose compared to those without. **(E)** Addition of glucose prevented the increased dextran permeability caused by hypoxia. **(F)** Representative images of tight junction ZO-1 staining in cells exposed to hypoxia for 16 hrs with or without glucose. Hypoxia-induced tight junctional disruption and cell detachment (asterisks) was prevented by glucose. **(B-E)** **P*<0.05 *vs*. respective Nx groups; $^{\#}P$<0.05 *vs*. 'Hx+Φ'. (n=6/group)**.**

Figure 17

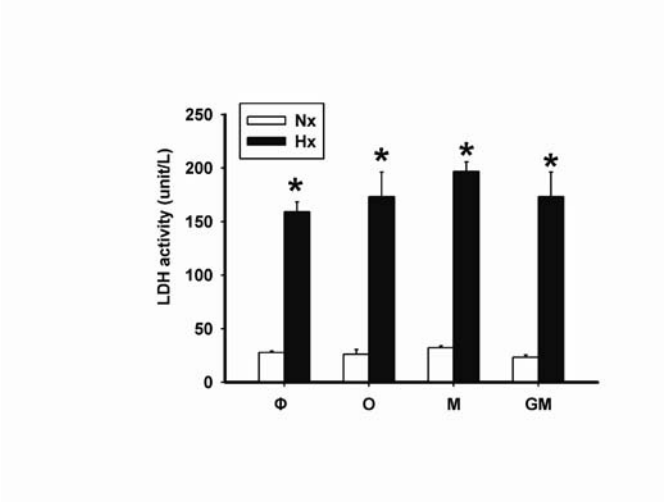

Figure 17 Addition of sugar analogs or amino acid did not reduce hypoxia-induced necrosis. The inhibition of hypoxia-induced LDH leakage was not seen by addition of 3-OMG (O), mannitol (M), or glutamate (GM). $P<0.05$ *vs*. Nx+Φ. (n=8/group).

Figure 18

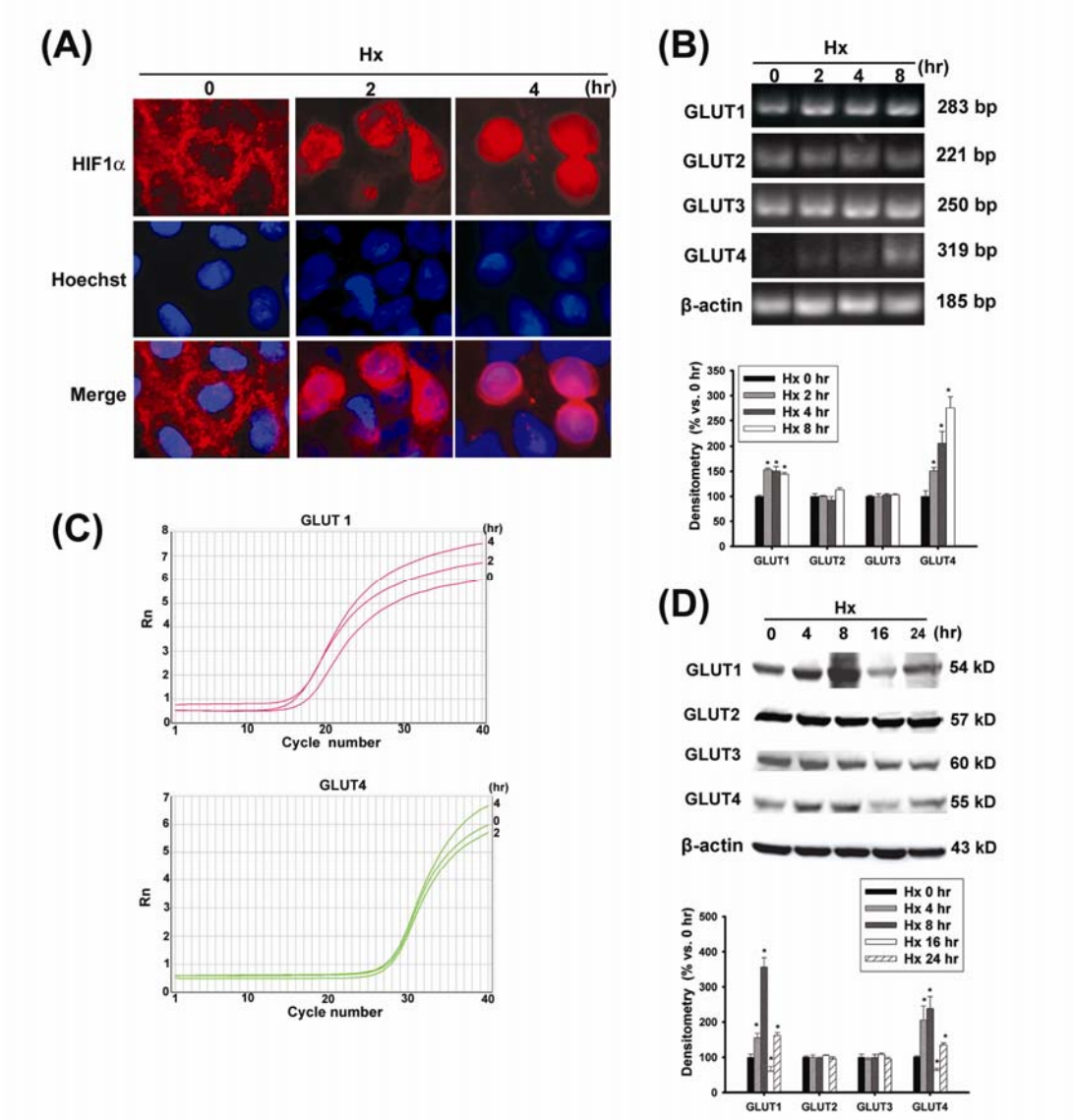

Figure 18 Hypoxic challenge induced HIF1α activation and hypoxia-targeted gene (GLUT-1 and -4) expression in the presence of glucose. (A) Representative immunofluorescence staining of HIF1α in hypoxic cells given glucose for 0, 2 and 4 hrs. Superimposed images of HIF1α staining (red) merged with cell nucleus (blue) showed cytoplasmic distribution of HIF1α under normoxic conditions and nuclear translocation of HIF-1α after hypoxic challenge for 2 and 4 hrs (n=6/group). **(B)** The mRNA levels of GLUT-1, -2, -3 and -4 following hypoxic challenge as determined by semiquantitative PCR analysis. **(C)** Representative quantification of mRNA expression of GLUT-1 and -4 in hypoxic cells by real-time PCR. **(D)** The protein levels of GLUT-1, -2, -3 and -4 after hypoxic challenge as determined by Western blots. **(B and D)** **P*<0.05 *vs*. '0 hr'. (n=4/group)

Figure 19

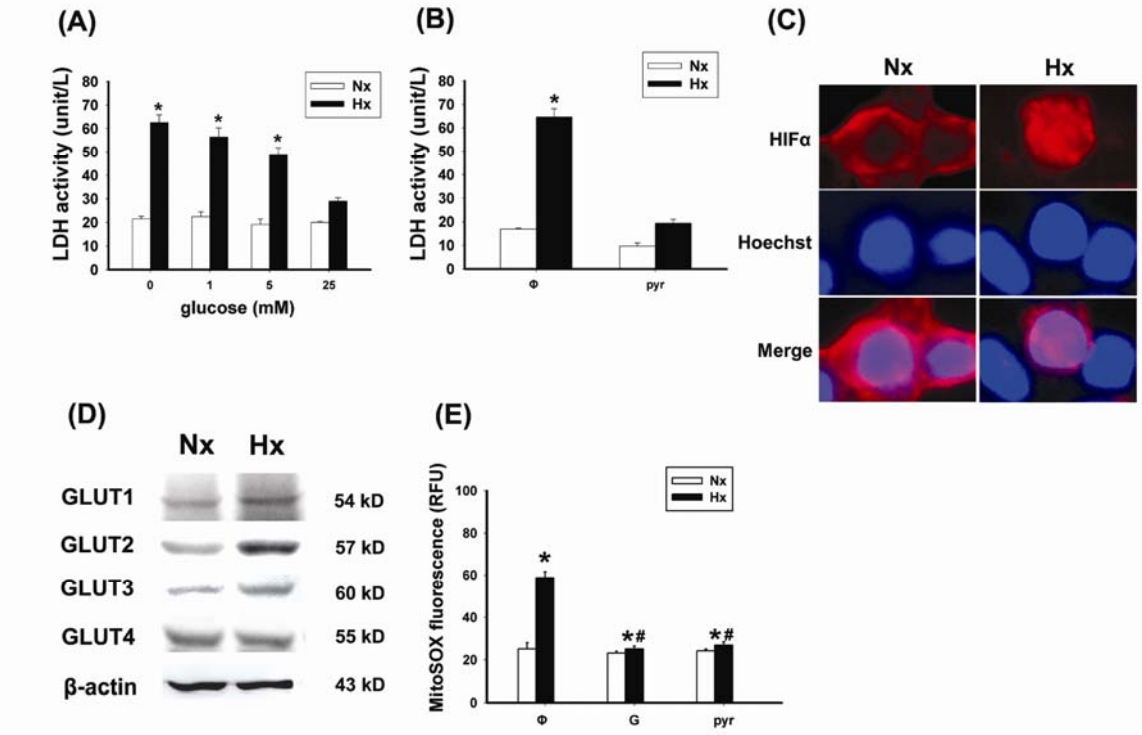

Figure 19 Resistance to hypoxia-induced necrosis is conferred by glycolytic pyruvate scavenging of mitochondrial superoxide in HT29 cells. (A) Various concentrations (0, 1, 5, and 25 mM) of glucose were added to hypoxic cells, and the LDH activity in the cell media was measured. **P*<0.05 *vs*. Nx at 0 mM. **(B)** Cells were normoxia and hypoxia exposed in the absence (Φ) or presence of ethyl pyruvate (pyr; 25 mM), and the LDH activity in cell media was measured. **P*<0.05 *vs*. respective Nx+Φ groups. (n=8/group). **(C)** Representative immunofluorescence staining of HIF1α in HT29 cells exposed to normoxia or hypoxia with glucose. Superimposed images of HIF1α staining (red) merged with cell nucleus (blue) showed cytoplasmic distribution of HIF1α under normoxic conditions and nuclear translocation of HIF1α after hypoxia (n=6/group). **(D)** The protein levels of GLUT-1, -2, -3 and -4 following exposure to normoxia or hypoxia. (n=3-4/group) **(E)** Addition of glucose decreased mitochondrial ROS levels in hypoxic HT29 cells. Replacing glucose with a pyruvate derivative (pyr) also reduced mitochondrial ROS in hypoxic cells. **P*<0.05 *vs*. respective Nx groups; $^{\#}P$<0.05 *vs*. Hx+Φ (n=8/group).

Figure 20

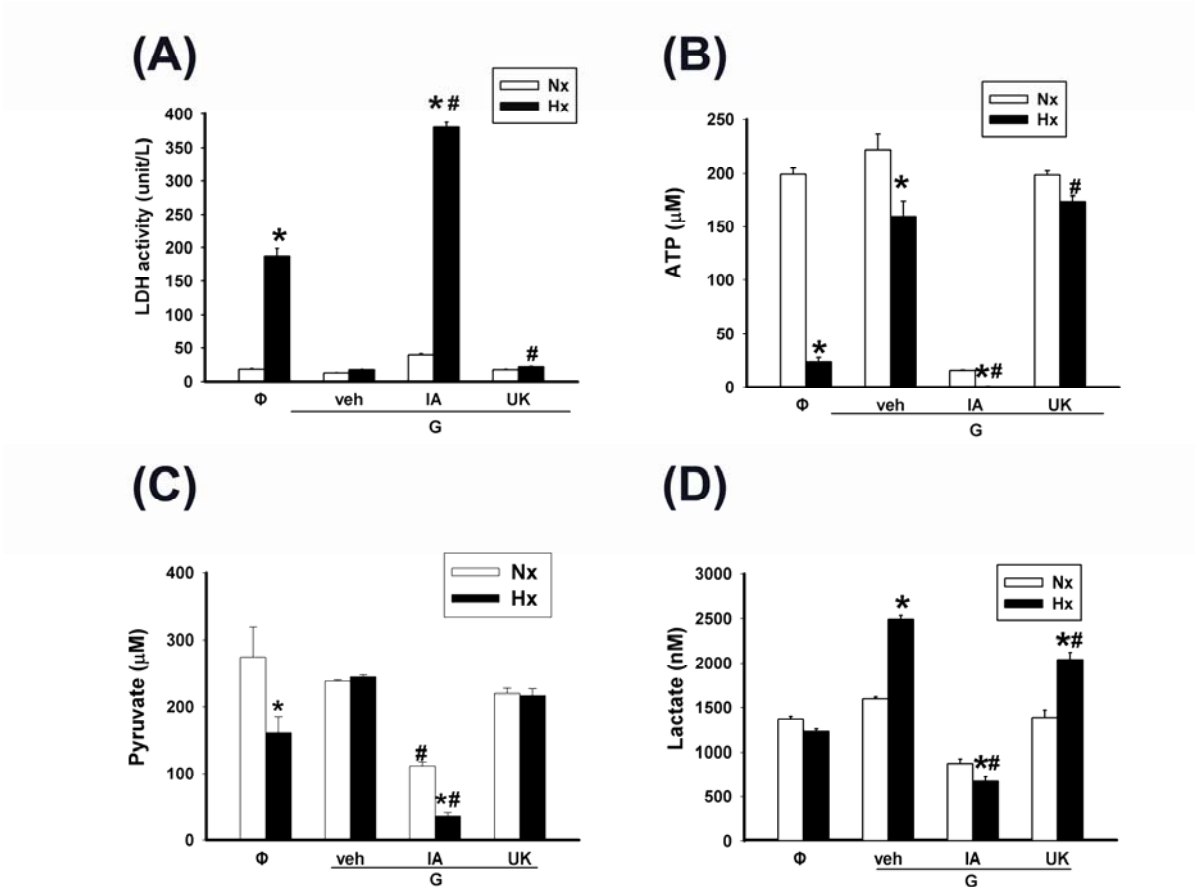

Figure 20 Anti-necrotic resistance of human colonic carcinoma cells was associated with anaerobic glycolytic metabolism. Cells were pretreated with vehicle (veh), iodoacetate (IA, 1 mM; a glycolytic inhibitor to GPD), or UK5099 (UK, 10 μM; a MPC inhibitor) prior to hypoxic challenge in the presence of glucose. The LDH activity in cell media **(A)**, and the intracellular levels of ATP **(B)**, pyruvate **(C)**, and lactate **(D)** were measured. **P*<0.05 *vs*. respective Nx groups; $^{\#}$*P*<0.05 *vs*. 'veh'. (n=8/group)

Figure 21

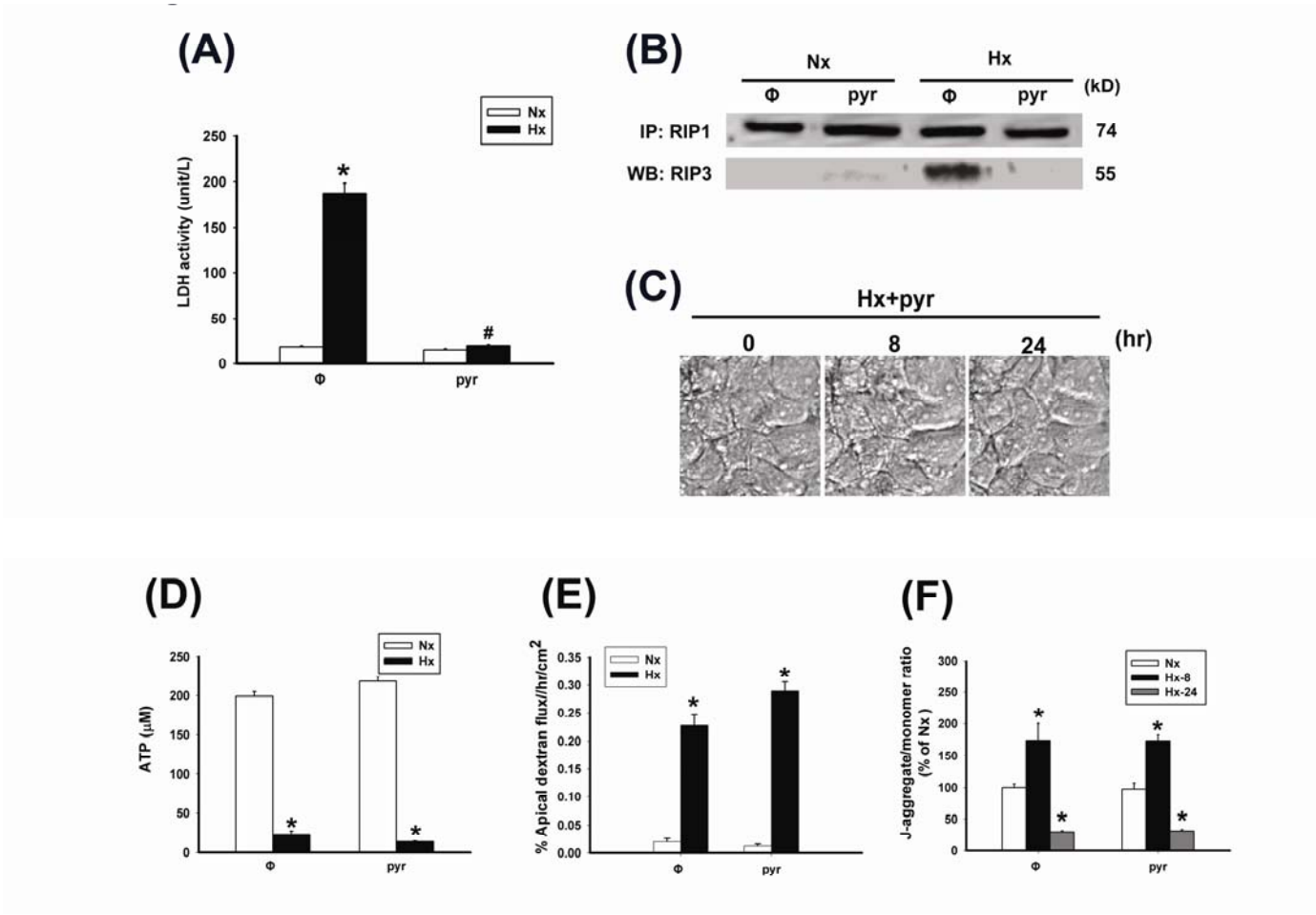

Figure 21 Pyruvate inhibited hypoxia-induced necrotic death in an energy-independent mechanism. Colonic cancer cells were normoxia and hypoxia exposed in the absence (Φ) or presence of ethyl pyruvate (pyr; 25 mM). Addition of pyruvate derivative prevented the LDH leakage **(A),** RIP1/3 complex formation **(B),** and morphological damage **(C)** caused by hypoxia. However, the cellular ATP levels **(D)**, barrier function **(E)**, and mitochondrial transmembrane potential **(F)** were not restored by pyruvate. **(A, D, E, and F)** **P*<0.05 *vs*. respective Nx groups; $^{\#}P$<0.05 *vs*. 'Hx+Φ'. (**A and D**, n=8/group; **B, C, E, and F,** n=4/group)

Figure 22

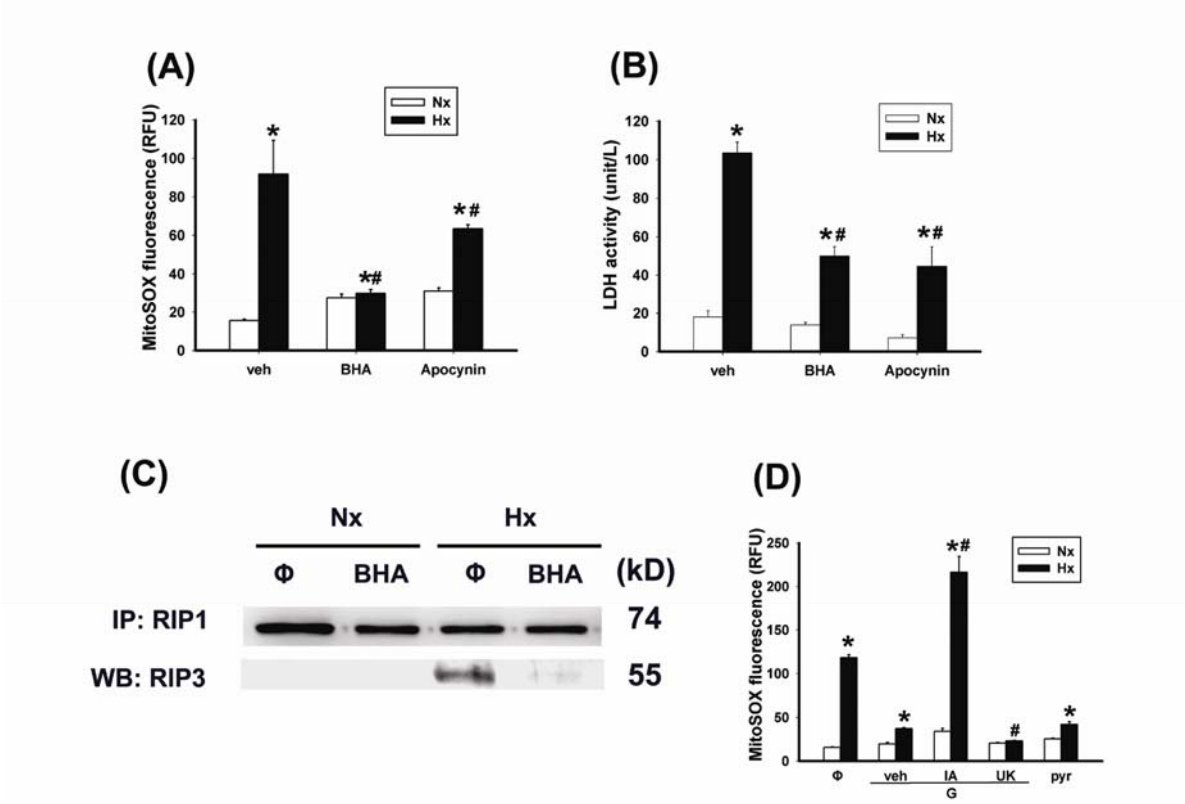

Figure 22 Pyruvate-mediated mitochondrial superoxide scavenging plays a critical role in resistance to hypoxia-induced necroptosis. (A) Increased MitoSOX fluorescence units were seen in hypoxic cells at the 8-hr time point, suggesting mitochondrial superoxide production upon hypoxic stress. The generation of mitochondrial ROS may be partially prevented by antioxidants (200 μM BHA or 1 mM apocynin), whereas vehicle control (veh) had no effect. **P*<0.05 *vs*. respective Nx groups; $^{\#}P$<0.05 *vs*. 'veh' (n=8/group). **(B)** The hypoxia-induced LDH leakage was abolished by pretreatment with antioxidants, suggesting that cell necrosis was dependent on mitochondrial ROS production. **P*<0.05 *vs*. respective Nx groups; $^{\#}P$<0.05 *vs*. 'veh' (n=8/group). **(C)** Immunoprecipitation blots showing the formation of RIP1/3 complex in hypoxic cells, which was inhibited by BHA. The experiments were repeated twice and similar results were obtained. (n=3/group). **(D)** Supplementation of glucose decreased mitochondrial ROS levels in hypoxic cells, which was reversed by pretreatment with iodoacetate (IA, 1 mM), but not UK5099 (UK, 10 μM) or vehicle (veh). Replacing glucose with a pyruvate derivative (pyr) also reduced mitochondrial ROS in hypoxic cells. **P*<0.05 *vs*. respective Nx groups; $^{\#}P$<0.05 *vs*. 'veh'. (n=8/group)

Figure 23

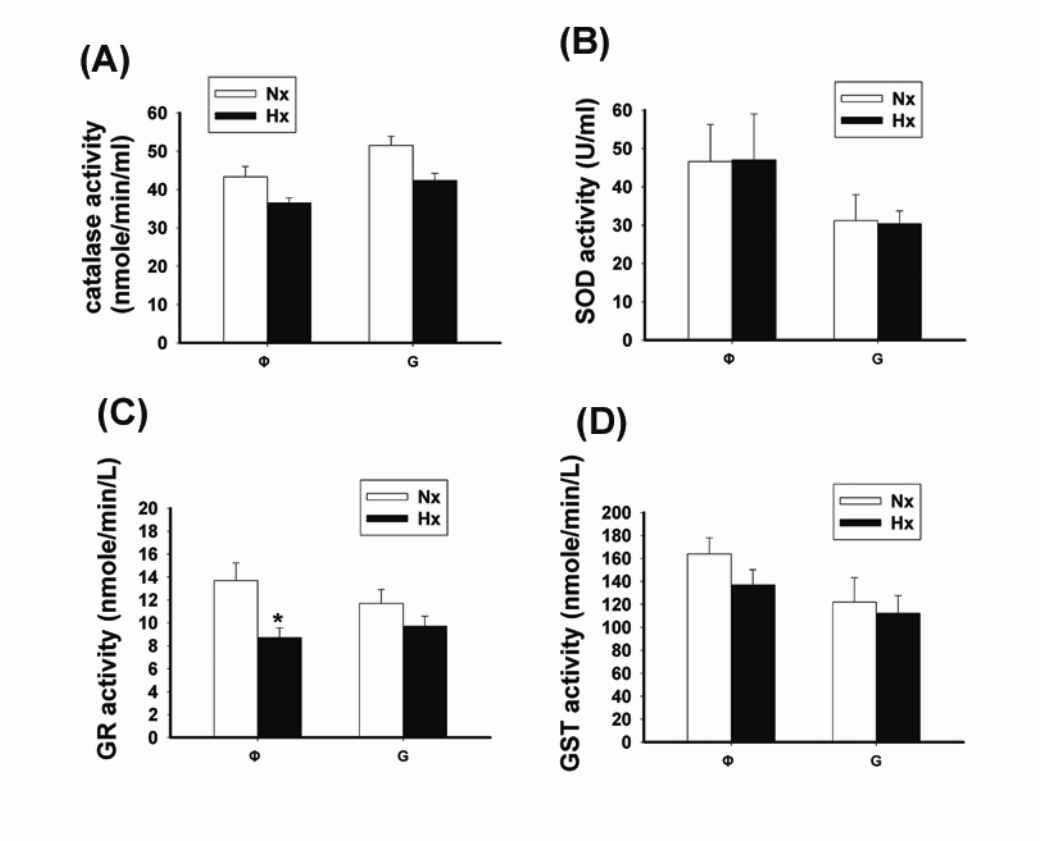

Figure 23 Supplementation of glucose did not alter the activities of redox enzymes in normoxic and hypoxic cells. The activities of **(A)** catalase, **(B)** superoxide dismutase (SOD), **(C)** glutathione reductase (GR), or **(D)** glutathione-S-transferase (GST), were measured in cells exposed to normoxia (Nx) and hypoxia (Hx) for 8 hrs in media containing 0 mM (Φ) or 25 mM of glucose (G). All of the enzyme activities were comparable between 'Hx+G' and 'Hx+Φ' cells. These results suggest that the cytoprotective effect exerted by glucose was not through redox mechanism. The GR activity in 'Hx+Φ' cells was lower than 'Nx+Φ' groups, suggesting that hypoxic challenge may decrease the GR activity in the absence of glucose. **P*<0.05 *vs*. Nx+Φ. (n=8/group).

Figure 24

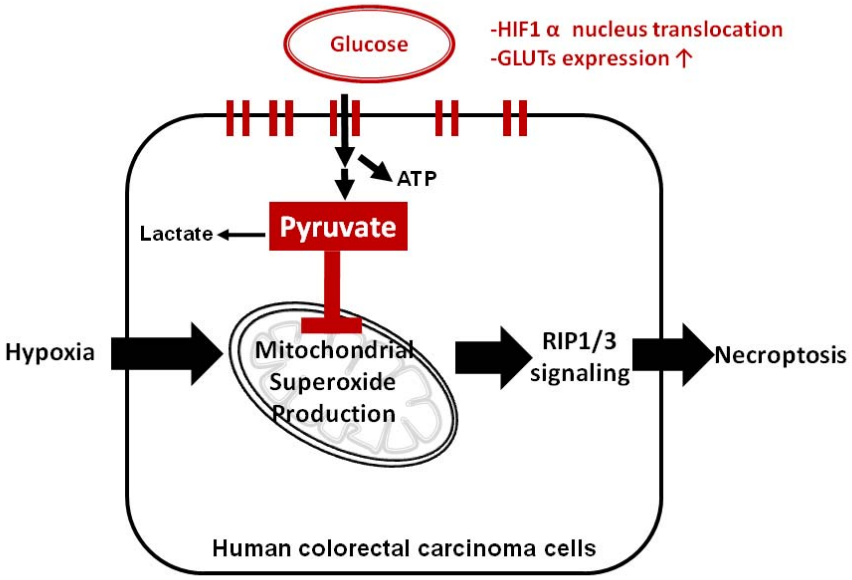

Figure 24 Schema of the resistance to necroptotic cell death induced by hypoxia in colorectal cancer is conferred by glycolytic pyruvate scavenging of mitochondrial superoxide.

Chapter 6 CONCLUDING REMARKS

Epithelial cells in the gastrointestinal tract have a highly turnover rate and play essential roles in maintaining gut homeostasis. In the current studies, both types of cell death, apoptosis and necroptosis, in epithelial cells may be attenuated by enteral glucose uptake. Normal SGLT1-mediated anti-apoptotic signaling may prevent epithelial cell death from ischemic stress in small intestine, but abnormal expression of GLUTs and enhanced glycolytic metabolism may also block hypoxic death in colorectal cancer cells.

The benefits of early enteral nutrition (EN) over parenteral supplementation and of preoperative oral carbohydrate loading (CHO) compared to overnight fasting have gained much attention in nutrition therapy nowadays (Fearon et al., 2005; Martindale et al., 2006). The advantage of early EN and CHO may also involve SGLT1-mediated nutritive and non-nutritive functions. On the other hand, drug resistance and metastatic transition in colorectal cancer are associated to adaptive responses to hypoxic microenvironment and HIF1-targeted increase of glucose transporters and glycolytic enzymes (Denko, 2008; Chiacchiera et al., 2009; Marin-Hernandez et al., 2009; Zeng et al., 2010; Rapisarda et al., 2012). Our study provided novel cancer killing strategies to be based on modulation of anaerobic glucose metabolism and glycolytic pyruvate in death resistance by targeting site-specific glucose transporters. The combinational

strategies with glucose- or pyruvate-targeted therapy may overcome the resistance to antiangiogesis or hypoxic stress.

In conclusion, the understanding of hypoxic-induced cell death pathways and resistance mechanisms conferred by glucose may benefit the development of novel therapeutic interventions targeting glucose transporters for treating gastrointestinal disease caused by abnormal cell death.

REFERENCE

Aban, N., L. Cinel, et al. (2005). "Ischemic preconditioning reduces caspase-related intestinal apoptosis." Surg Today **35**(3): 228-234.

Airley, R., A. Evans, et al. (2010). "Glucose transporter Glut-1 is detectable in peri-necrotic regions in many human tumor types but not normal tissues: Study using tissue microarrays." Ann Anat **192**(3): 133-138.

Bai, D., L. Ueno, et al. (2009). "Akt-mediated regulation of NFkappaB and the essentialness of NFkappaB for the oncogenicity of PI3K and Akt." Int J Cancer **125**(12): 2863-2870.

Becker, L. B., T. L. vanden Hoek, et al. (1999). "Generation of superoxide in cardiomyocytes during ischemia before reperfusion." Am J Physiol **277**(6 Pt 2): H2240-2246.

Berghe, T. V., N. Vanlangenakker, et al. (2010). "Necroptosis, necrosis and secondary necrosis converge on similar cellular disintegration features." Cell Death Differ **17**(6): 922-930.

Bouchard, V., C. Harnois, et al. (2008). "B1 integrin/Fak/Src signaling in intestinal epithelial crypt cell survival: integration of complex regulatory mechanisms." Apoptosis **13**(4): 531-542.

Camara, A. K., M. Aldakkak, et al. (2007). "ROS scavenging before 27 degrees C ischemia protects hearts and reduces mitochondrial ROS, Ca2+ overload, and changes in redox state." Am J Physiol Cell Physiol **292**(6): C2021-2031.

Chakrabarti, G., X. Zhou, et al. (2003). "Death pathways activated in CaCo-2 cells by Clostridium perfringens enterotoxin." Infect Immun **71**(8): 4260-4270.

Chang, F., J. T. Lee, et al. (2003). "Involvement of PI3K/Akt pathway in cell cycle progression, apoptosis, and neoplastic transformation: a target for cancer chemotherapy." Leukemia **17**(3): 590-603.

Chang, J. X., S. Chen, et al. (2005). "Functional and morphological changes of the gut barrier during the restitution process after hemorrhagic shock." World J Gastroenterol **11**(35): 5485-5491.

Chiacchiera, F., A. Matrone, et al. (2009). "p38alpha blockade inhibits colorectal cancer growth in vivo by inducing a switch from HIF1alpha- to FoxO-dependent transcription." Cell Death Differ **16**(9): 1203-1214.

Cho, Y. S., S. Challa, et al. (2009). "Phosphorylation-driven assembly of the RIP1-RIP3 complex regulates programmed necrosis and virus-induced inflammation." Cell **137**(6): 1112-1123.

Colgan, S. P. and C. T. Taylor (2010). "Hypoxia: an alarm signal during intestinal inflammation." Nat Rev Gastroenterol Hepatol **7**(5): 281-287.

Dan, H. C. and A. S. Baldwin (2008). "Differential involvement of IkappaB kinases alpha and beta in cytokine- and insulin-induced mammalian target of rapamycin activation determined by Akt." J Immunol **180**(11): 7582-7589.

Danial, N. N. (2008). "BAD: undertaker by night, candyman by day." Oncogene **27 Suppl 1**: S53-70.

Danial, N. N., C. F. Gramm, et al. (2003). "BAD and glucokinase reside in a mitochondrial complex that integrates glycolysis and apoptosis." Nature **424**(6951): 952-956.

de Wit, M., C. R. Jimenez, et al. (2012). "Cell surface proteomics identifies glucose transporter type 1 and prion protein as candidate biomarkers for colorectal adenoma-to-carcinoma progression." Gut **61**(6): 855-864.

Declercq, W., T. Vanden Berghe, et al. (2009). "RIP kinases at the crossroads of cell death and survival." Cell **138**(2): 229-232.

Denko, N. C. (2008). "Hypoxia, HIF1 and glucose metabolism in the solid tumour." Nat Rev Cancer **8**(9): 705-713.

Dufort, F. J., B. F. Bleiman, et al. (2007). "Cutting edge: IL-4-mediated protection of primary B lymphocytes from apoptosis via Stat6-dependent regulation of glycolytic metabolism." J Immunol **179**(8): 4953-4957.

Egan, L. J., L. Eckmann, et al. (2004). "IkappaB-kinasebeta-dependent NF-kappaB activation provides radioprotection to the intestinal epithelium." Proc Natl Acad Sci U S A **101**(8): 2452-2457.

Fearon, K. C., O. Ljungqvist, et al. (2005). "Enhanced recovery after surgery: a consensus review of clinical care for patients undergoing colonic resection." Clin Nutr **24**(3): 466-477.

Fleming, S. E., K. L. Zambell, et al. (1997). "Glucose and glutamine provide similar proportions of energy to mucosal cells of rat small intestine." Am J Physiol **273**(4 Pt 1): G968-978.

Funda, D. P., L. Tuckova, et al. (2001). "CD14 is expressed and released as soluble CD14 by human intestinal epithelial cells in vitro: lipopolysaccharide activation of epithelial cells revisited." Infect Immun **69**(6): 3772-3781.

Garedew, A., S. O. Henderson, et al. (2010). "Activated macrophages utilize glycolytic ATP to maintain mitochondrial membrane potential and prevent apoptotic cell death." Cell Death Differ **17**(10): 1540-1550.

Godoy, A., V. Ulloa, et al. (2006). "Differential subcellular distribution of glucose transporters GLUT1-6 and GLUT9 in human cancer: ultrastructural localization of GLUT1 and GLUT5 in breast tumor tissues." J Cell Physiol **207**(3): 614-627.

Goossens, V., J. Grooten, et al. (1995). "Direct evidence for tumor necrosis factor-induced mitochondrial reactive oxygen intermediates and their involvement in cytotoxicity." Proc Natl Acad Sci U S A **92**(18): 8115-8119.

Greijer, A. E., P. M. Delis-van Diemen, et al. (2008). "Presence of HIF-1 and related genes in normal mucosa, adenomas and carcinomas of the colorectum." Virchows Arch **452**(5): 535-544.

Gunther, C., E. Martini, et al. (2011). "Caspase-8 regulates TNF-alpha-induced epithelial necroptosis and terminal ileitis." Nature **477**(7364): 335-339.

Guo, G. F., Y. C. Cai, et al. (2011). "Overexpression of SGLT1 and EGFR in colorectal cancer showing a correlation with the prognosis." Med Oncol **28 Suppl 1**: S197-203.

Hall, J. L., J. C. Chatham, et al. (2001). "Upregulation of glucose metabolism during intimal lesion formation is coupled to the inhibition of vascular smooth muscle cell apoptosis. Role of GSK3beta." Diabetes **50**(5): 1171-1179.

Hawley, D. J., F. Wolfe, et al. (1992). "The sense of coherence questionnaire in patients with rheumatic

disorders." J Rheumatol **19**(12): 1912-1918.

Hayashi, M., M. Sakata, et al. (2004). "Induction of glucose transporter 1 expression through hypoxia-inducible factor 1alpha under hypoxic conditions in trophoblast-derived cells." J Endocrinol **183**(1): 145-154.

He, S., L. Wang, et al. (2009). "Receptor interacting protein kinase-3 determines cellular necrotic response to TNF-alpha." Cell **137**(6): 1100-1111.

Herzig, S., E. Raemy, et al. (2012). "Identification and functional expression of the mitochondrial pyruvate carrier." Science **337**(6090): 93-96.

Higa, O. H., E. R. Parra, et al. (2007). "Protective effects of ascorbic acid pretreatment in a rat model of intestinal ischemia-reperfusion injury: a histomorphometric study." Clinics (Sao Paulo) **62**(3): 315-320.

Hildyard, J. C., C. Ammala, et al. (2005). "Identification and characterisation of a new class of highly specific and potent inhibitors of the mitochondrial pyruvate carrier." Biochim Biophys Acta **1707**(2-3): 221-230.

Hsiao, J. K., C. Y. Huang, et al. (2009). "Magnetic resonance imaging detects intestinal barrier dysfunction in a rat model of acute mesenteric ischemia/reperfusion injury." Invest Radiol **44**(6): 329-335.

Huang, C. Y., J. K. Hsiao, et al. (2011). "Anti-apoptotic PI3K/Akt signaling by sodium/glucose transporter 1 reduces epithelial barrier damage and bacterial translocation in intestinal ischemia." Lab Invest **91**(2): 294-309.

Huang, C. Y., W. T. Kuo, et al. (2013). "Resistance to hypoxia-induced necroptosis is conferred by glycolytic pyruvate scavenging of mitochondrial superoxide in colorectal cancer cells." Cell Death Dis **4**: e622.

Hunter, C. J., B. Podd, et al. (2008). "Evidence vs experience in neonatal practices in necrotizing enterocolitis." J Perinatol **28 Suppl 1**: S9-S13.

Jaakkola, P., D. R. Mole, et al. (2001). "Targeting of HIF-alpha to the von Hippel-Lindau ubiquitylation complex by O2-regulated prolyl hydroxylation." Science **292**(5516): 468-472.

Jilling, T., D. Simon, et al. (2006). "The roles of bacteria and TLR4 in rat and murine models of necrotizing enterocolitis." J Immunol **177**(5): 3273-3282.

Kalda, A., E. Eriste, et al. (1998). "Medium transitory oxygen-glucose deprivation induced both apoptosis and necrosis in cerebellar granule cells." Neurosci Lett **240**(1): 21-24.

Kalischuk, L. D., G. D. Inglis, et al. (2007). "Strain-dependent induction of epithelial cell oncosis by Campylobacter jejuni is correlated with invasion ability and is independent of cytolethal distending toxin." Microbiology **153**(Pt 9): 2952-2963.

Kao, K. K. and M. P. Fink (2010). "The biochemical basis for the anti-inflammatory and cytoprotective actions of ethyl pyruvate and related compounds." Biochem Pharmacol **80**(2): 151-159.

Kellett, G. L. (2001). "The facilitated component of intestinal glucose absorption." J Physiol **531**(Pt 3): 585-595.

Kellett, G. L. and P. A. Helliwell (2000). "The diffusive component of intestinal glucose absorption is mediated by the glucose-induced recruitment of GLUT2 to the brush-border membrane." Biochem J **350 Pt 1**: 155-162.

Khanna, A., J. E. Rossman, et al. (2001). "Intestinal and hemodynamic impairment following mesenteric ischemia/reperfusion." J Surg Res **99**(1): 114-119.

Kles, K. A., J. R. Turner, et al. (2002). "2001 Harry M. Vars Research Award. Enteral nutrients alter enterocyte function within an in vitro model similar to an acute in vivo rat model during hypoxia." JPEN J Parenter Enteral Nutr **26**(2): 71-76.

Kondo, S., S. Y. Seo, et al. (2006). "EBV latent membrane protein 1 up-regulates hypoxia-inducible factor 1alpha through Siah1-mediated down-regulation of prolyl hydroxylases 1 and 3 in nasopharyngeal epithelial cells." Cancer Res **66**(20): 9870-9877.

Laukoetter, M. G., M. Bruewer, et al. (2006). "Regulation of the intestinal epithelial barrier by the apical junctional complex." Curr Opin Gastroenterol **22**(2): 85-89.

Liang, J. and J. M. Slingerland (2003). "Multiple roles of the PI3K/PKB (Akt) pathway in cell cycle progression." Cell Cycle **2**(4): 339-345.

LoPiccolo, J., G. M. Blumenthal, et al. (2008). "Targeting the PI3K/Akt/mTOR pathway: effective combinations and clinical considerations." Drug Resist Updat **11**(1-2): 32-50.

Mallick, I. H., W. Yang, et al. (2004). "Ischemia-reperfusion injury of the intestine and protective strategies against injury." Dig Dis Sci **49**(9): 1359-1377.

Marin-Hernandez, A., J. C. Gallardo-Perez, et al. (2009). "HIF-1alpha modulates energy metabolism in cancer cells by inducing over-expression of specific glycolytic isoforms." Mini Rev Med Chem **9**(9): 1084-1101.

Martindale, R. G. and L. L. Maerz (2006). "Management of perioperative nutrition support." Curr Opin Crit Care **12**(4): 290-294.

Marxsen, J. H., P. Stengel, et al. (2004). "Hypoxia-inducible factor-1 (HIF-1) promotes its degradation by induction of HIF-alpha-prolyl-4-hydroxylases." Biochem J **381**(Pt 3): 761-767.

Matsushita, K., K. Uchida, et al. (2012). "Glycolysis inhibitors as a potential therapeutic option to treat aggressive neuroblastoma expressing GLUT1." J Pediatr Surg **47**(7): 1323-1330.

Mayer, B. and R. Oberbauer (2003). "Mitochondrial regulation of apoptosis." News Physiol Sci **18**: 89-94.

Meurette, O., A. Rebillard, et al. (2007). "TRAIL induces receptor-interacting protein 1-dependent and caspase-dependent necrosis-like cell death under acidic extracellular conditions." Cancer Res **67**(1): 218-226.

Millonig, G., S. Hegedusch, et al. (2009). "Hypoxia-inducible factor 1 alpha under rapid enzymatic hypoxia: cells sense decrements of oxygen but not hypoxia per se." Free Radic Biol Med **46**(2): 182-191.

Murphy, A. J., P. M. Guyre, et al. (2010). "Estradiol suppresses NF-kappa B activation through coordinated regulation of let-7a and miR-125b in primary human macrophages." J Immunol

184(9): 5029-5037.

Nenci, A., C. Becker, et al. (2007). "Epithelial NEMO links innate immunity to chronic intestinal inflammation." Nature **446**(7135): 557-561.

Nilsson, U. A., M. H. Schoenberg, et al. (1994). "Free radicals and pathogenesis during ischemia and reperfusion of the cat small intestine." Gastroenterology **106**(3): 629-636.

Noguchi, Y., T. Okamoto, et al. (2000). "Expression of facilitative glucose transporter 1 mRNA in colon cancer was not regulated by k-ras." Cancer Lett **154**(2): 137-142.

Ouiddir, A., C. Planes, et al. (1999). "Hypoxia upregulates activity and expression of the glucose transporter GLUT1 in alveolar epithelial cells." Am J Respir Cell Mol Biol **21**(6): 710-718.

Palazzo, M., S. Gariboldi, et al. (2008). "Sodium-dependent glucose transporter-1 as a novel immunological player in the intestinal mucosa." J Immunol **181**(5): 3126-3136.

Potoka, D. A., E. P. Nadler, et al. (2000). "Inhibition of NF-kappaB by IkappaB prevents cytokine-induced NO production and promotes enterocyte apoptosis in vitro." Shock **14**(3): 366-373.

Ramachandran, A., M. Madesh, et al. (2000). "Apoptosis in the intestinal epithelium: its relevance in normal and pathophysiological conditions." J Gastroenterol Hepatol **15**(2): 109-120.

Rapisarda, A. and G. Melillo (2012). "Overcoming disappointing results with antiangiogenic therapy by targeting hypoxia." Nat Rev Clin Oncol **9**(7): 378-390.

Russo, V. C., K. Kobayashi, et al. (2004). "Neuronal protection from glucose deprivation via modulation of glucose transport and inhibition of apoptosis: a role for the insulin-like growth factor system." Brain Res **1009**(1-2): 40-53.

Selvaraj, S. K. and N. V. Prasadarao (2005). "Escherichia coli K1 inhibits proinflammatory cytokine induction in monocytes by preventing NF-kappaB activation." J Leukoc Biol **78**(2): 544-554.

Shahrzad, S., L. Quayle, et al. (2005). "Ischemia-induced K-ras mutations in human colorectal cancer cells: role of microenvironmental regulation of MSH2 expression." Cancer Res **65**(18): 8134-8141.

Shimizu, S., M. Narita, et al. (1999). "Bcl-2 family proteins regulate the release of apoptogenic cytochrome c by the mitochondrial channel VDAC." Nature **399**(6735): 483-487.

Shiue, H., M. W. Musch, et al. (2005). "Akt2 phosphorylates ezrin to trigger NHE3 translocation and activation." J Biol Chem **280**(2): 1688-1695.

Soop, M., J. Nygren, et al. (2004). "Preoperative oral carbohydrate treatment attenuates endogenous glucose release 3 days after surgery." Clin Nutr **23**(4): 733-741.

Stiehl, D. P., R. Wirthner, et al. (2006). "Increased prolyl 4-hydroxylase domain proteins compensate for decreased oxygen levels. Evidence for an autoregulatory oxygen-sensing system." J Biol Chem **281**(33): 23482-23491.

Sun, D., N. Nguyen, et al. (1994). "Ischemia induces translocation of the insulin-responsive glucose transporter GLUT4 to the plasma membrane of cardiac myocytes." Circulation **89**(2): 793-798.

Sun, Z., X. Wang, et al. (1998). "The influence of intestinal ischemia and reperfusion on bidirectional

intestinal barrier permeability, cellular membrane integrity, proteinase inhibitors, and cell death in rats." Shock **10**(3): 203-212.

Suzuki, M., T. Hisamatsu, et al. (2003). "Gamma interferon augments the intracellular pathway for lipopolysaccharide (LPS) recognition in human intestinal epithelial cells through coordinated up-regulation of LPS uptake and expression of the intracellular Toll-like receptor 4-MD-2 complex." Infect Immun **71**(6): 3503-3511.

Temkin, V., Q. Huang, et al. (2006). "Inhibition of ADP/ATP exchange in receptor-interacting protein-mediated necrosis." Mol Cell Biol **26**(6): 2215-2225.

Torres, M. P., S. Rachagani, et al. (2012). "Graviola: a novel promising natural-derived drug that inhibits tumorigenicity and metastasis of pancreatic cancer cells in vitro and in vivo through altering cell metabolism." Cancer Lett **323**(1): 29-40.

Turner, J. R. (2009). "Intestinal mucosal barrier function in health and disease." Nat Rev Immunol **9**(11): 799-809.

Turrens, J. F. (2003). "Mitochondrial formation of reactive oxygen species." J Physiol **552**(Pt 2): 335-344.

Urbich, C., A. Knau, et al. (2005). "FOXO-dependent expression of the proapoptotic protein Bim: pivotal role for apoptosis signaling in endothelial progenitor cells." FASEB J **19**(8): 974-976.

Vincenti, M., M. Behrends, et al. (2010). "Induction of intestinal ischemia reperfusion injury by portal vein outflow occlusion in rats." J Gastroenterol **45**(11): 1103-1110.

Wang, W., N. Smail, et al. (1998). "Increased gut permeability after hemorrhage is associated with upregulation of local and systemic IL-6." J Surg Res **79**(1): 39-46.

Warburg, O. (1956). "On respiratory impairment in cancer cells." Science **124**(3215): 269-270.

Welz, P. S., A. Wullaert, et al. (2011). "FADD prevents RIP3-mediated epithelial cell necrosis and chronic intestinal inflammation." Nature **477**(7364): 330-334.

Wofford, J. A., H. L. Wieman, et al. (2008). "IL-7 promotes Glut1 trafficking and glucose uptake via STAT5-mediated activation of Akt to support T-cell survival." Blood **111**(4): 2101-2111.

Wu, B., A. Ootani, et al. (2004). "Ischemic preconditioning attenuates ischemia-reperfusion-induced mucosal apoptosis by inhibiting the mitochondria-dependent pathway in rat small intestine." Am J Physiol Gastrointest Liver Physiol **286**(4): G580-587.

Wu, L. L., H. D. Chiu, et al. (2011). "Epithelial inducible nitric oxide synthase causes bacterial translocation by impairment of enterocytic tight junctions via intracellular signals of Rho-associated kinase and protein kinase C zeta." Crit Care Med **39**(9): 2087-2098.

Xu, R. H., H. Pelicano, et al. (2005). "Inhibition of glycolysis in cancer cells: a novel strategy to overcome drug resistance associated with mitochondrial respiratory defect and hypoxia." Cancer Res **65**(2): 613-621.

Yasuhara, H. (2005). "Acute mesenteric ischemia: the challenge of gastroenterology." Surg Today **35**(3): 185-195.

Yeh, C. S., J. Y. Wang, et al. (2008). "Significance of the glycolytic pathway and glycolysis related-genes in tumorigenesis of human colorectal cancers." Oncol Rep **19**(1): 81-91.

Yu, L. C. (2010). "Protective mechanism against gut barrier dysfunction mesenteric ischemia/reperfusion." Adaptive Medicine **2**(1): 11-22.

Yu, L. C., A. N. Flynn, et al. (2005). "SGLT-1-mediated glucose uptake protects intestinal epithelial cells against LPS-induced apoptosis and barrier defects: a novel cellular rescue mechanism?" FASEB J **19**(13): 1822-1835.

Yu, L. C., C. Y. Huang, et al. (2008). "SGLT-1-mediated glucose uptake protects human intestinal epithelial cells against Giardia duodenalis-induced apoptosis." Int J Parasitol **38**(8-9): 923-934.

Yu, L. C., G. Montagnac, et al. (2003). "Intestinal epithelial CD23 mediates enhanced antigen transport in allergy: evidence for novel splice forms." Am J Physiol Gastrointest Liver Physiol **285**(1): G223-234.

Yu, L. C., J. R. Turner, et al. (2006). "LPS/CD14 activation triggers SGLT-1-mediated glucose uptake and cell rescue in intestinal epithelial cells via early apoptotic signals upstream of caspase-3." Exp Cell Res **312**(17): 3276-3286.

Yu, L. C., J. T. Wang, et al. (2012). "Host-microbial interactions and regulation of intestinal epithelial barrier function: From physiology to pathology." World J Gastrointest Pathophysiol **3**(1): 27-43.

Zeng, L., K. M. Biernacka, et al. (2010). "Hyperglycaemia confers resistance to chemotherapy on breast cancer cells: the role of fatty acid synthase." Endocr Relat Cancer **17**(2): 539-551.

Zhang, D. W., J. Shao, et al. (2009). "RIP3, an energy metabolism regulator that switches TNF-induced cell death from apoptosis to necrosis." Science **325**(5938): 332-336.

Zhao, H., H. Shiue, et al. (2004). "Ezrin regulates NHE3 translocation and activation after Na+-glucose cotransport." Proc Natl Acad Sci U S A **101**(25): 9485-9490.

Zheng, Y., Y. Shi, et al. (2004). "Essential role of the voltage-dependent anion channel (VDAC) in mitochondrial permeability transition pore opening and cytochrome c release induced by arsenic trioxide." Oncogene **23**(6): 1239-1247.

Zhou, Y., F. Tozzi, et al. (2012). "Intracellular ATP levels are a pivotal determinant of chemoresistance in colon cancer cells." Cancer Res **72**(1): 304-314.